Femtochemistry of Norrish Type-I Reactions: IV. Highly Excited Ketones—Experimental

Theis I. Sølling, Eric W.-G. Diau, Carsten Kötting, Steven De Feyter, and Ahmed H. Zewail*[a]

Femtosecond dynamics of Norrish type-I reactions of cyclic and acyclic ketones have been investigated in real time for a series of 13 compounds using femtosecond-resolved time-of-flight mass spectrometry. A general physical description of the ultrafast processes of ketones excited into a high-lying Rydberg state is presented. It accounts not only for the results that are presented herein but also for the results of previously reported studies. For highly excited ketones, we show that the Norrish type-I reaction is nonconcerted, and that the first bond breakage occurs along the effectively repulsive S_2 surface involving the C—C bond in a manner which is similar to that of ketones in the S_1 state (E. W.-G. Diau et al. ChemPhysChem ***2001***, 2, *273 – 293). The experimental results show that the wave packet motion out of the initial Franck – Condon region and down to the S_2 state can be resolved. This femtosecond (fs) internal conversion from the highly excited Rydberg state to the S_2 state proceeds through conical intersections (Rydberg – valence) that are accessed through the C=O stretching motion. In one of these conical intersections, the internal energy is guided into an asymmetric stretching mode. This explains the previously reported pronounced nonstatistical nature of the reaction. The second bond breakage involves an excited-state acyl radical and occurs on a time scale that is up to one order of magnitude longer than the first. We discuss the details regarding the ion chemistry, which determines the appearance of the mass spectra that arise from ionization on the fs time scale. The experimental results presented here, aided by the theoretical work reported in paper III, provide a unified picture of Norrish reactions on excited states and on the ground-state potential energy surfaces.*

KEYWORDS:

femtochemistry · conical intersections · transition states · Norrish reactions · mass spectrometry

1. Introduction

The photochemistry of ketones has been a research topic of great interest over the past decades, and it is well established that the major unimolecular decomposition pathway for ketones without hydrogen atoms at a γ-carbon is a simple cleavage of the carbonyl – alkyl C—C bond.[1] For example the reaction for acetone is given in Equation (1).

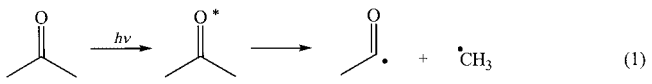

(1)

This process is commonly referred to as an α-cleavage or a Norrish type-I reaction.[1] The acetyl radical further decomposes to form carbon monoxide and a methyl radical. At high enough energies it is, in principle, possible to break both bonds in one step. Real-time studies of the elementary processes on the fs time scale have focused on the question of whether the decomposition is concerted or stepwise in nature and on the dynamics.[2–12] The reaction dynamics have been studied using a wide variety of wavelengths,[2–12] and acetone has been the prototypical example of a ketone in these investigations. The symmetry and energy of the electronic states of acetone are well established.[13–15] In particular, the complete active space (CAS) investigation by Roos and co-workers[13] and the time-dependant density functional theory (TDDFT) investigation by Wiberg et al.[15] have aided a complete assignment of the absorption spectrum.

In the introduction of our preceding paper (part III) in this issue,[16] we summarized the key results of the experimental and theoretical investigations of Norrish type-I reactions in ketones, on the ground-state surface and following excitation to S_1, S_2, and higher-energy states.[16] Here we shall not repeat this summary but focus on the unified mechanism that describes the vast amount of results on this class of reactions. There is now a general agreement that the Norrish type-I reaction is stepwise.[2, 3, 5–7, 9] However, the detailed mechanism for bond breakage from highly excited states is rather opaque. An elucidation would provide a more thorough understanding of the various time scales for bond breakage that have been observed and the forces which control the time scale and energy release.

[a] *Prof. A. H. Zewail, Dr. T. I. Sølling, Dr. E. W.-G. Diau, Dr. C. Kötting, Dr. S. De Feyter*
Arthur Amos Noyes Laboratory of Chemical Physics
California Institute of Technology
Pasadena, CA 91125, (USA)
Fax: (+1) 626-792-8456
http://www.its.caltech.edu/~femto/
E-mail: zewail@caltech.edu

In this work, the aim is to provide a general physical picture for the Norrish type-I reaction of highly excited ketones and to unify the available experimental results. For this purpose we investigated a series of 13 ketones in which the number of alkyl groups at the α-carbons was varied in a systematic manner (Figure 1). We address the relation to the previously reported

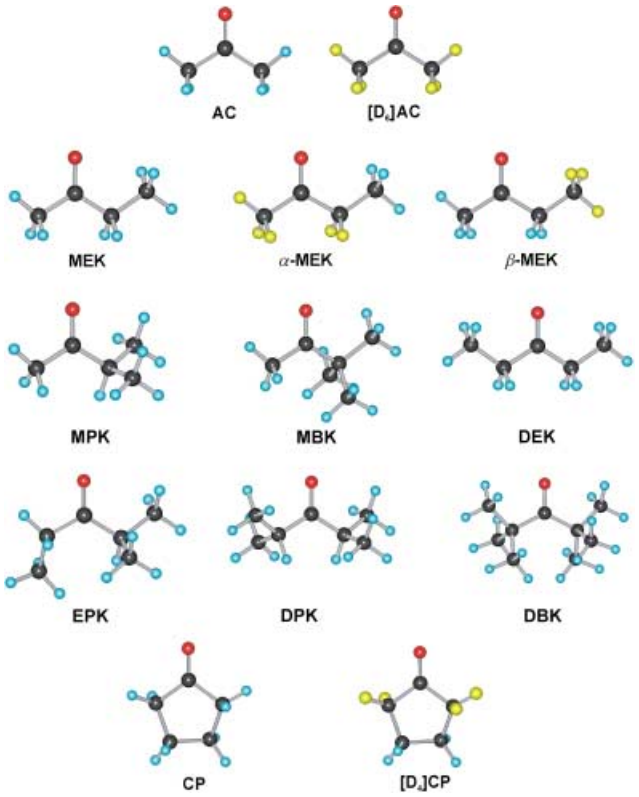

Figure 1. *The acyclic and cyclic ketones under study and their abbreviated names. The yellow spheres correspond to deuterium.*

results for excitations to S_1, S_2, and S_n[1–12, 17, 18] and compare with the theoretical findings of the preceding paper.[16] Furthermore, we elaborate on the results for the cyclic ketones[19, 20] and provide a more thorough understanding of why these reactions are highly nonstatistical in nature. Finally, we discuss details of the decomposition of the ionic species which result from the employed detection technique and rationalize the observed multiphoton-ionization mass spectra of the ketones studied.

Experimental Section

The fs laser and molecular beam apparatus have been described in detail elsewhere.[2, 21] Briefly, the output of a colliding-pulse, mode-locked oscillator (CPM) was amplified with a four-stage dye amplifier, pumped by a Nd:YAG laser at 20 Hz. The output, after recompression by a four prism setup, was typically a 80 fs width pulse with an intensity of $\sim$150 μJ pulse^{-1} at 615 nm. It was split to provide the pump and probe pulses; for the pump, the 615 nm output was frequency doubled whereas it was passed directly to a computer-controlled translation stage for the time delay and was used as probe in that manner. The time zero was measured in situ, using xenon ionization as a reference.[22]

The pump and probe pulses were spatially combined and focussed onto the supersonic molecular beam apparatus containing the time-of-flight mass spectrometer. Both pump and probe pulses were appropriately attenuated to minimize background signals and the ratio between the intensities of the pump and probe pulses was chosen such that the absorption of two pump photons is dominant. By gating the signal due to a particular ion, the temporal evolution of each species was measured. For the systems discussed, the dependence of the ion current (S) on the pump intensity (I) confirmed that the pump process involves the absorption of two photons (186 kcal mol^{-1}).

This was confirmed for all the parent transients at a 50 fs time delay as well as for some fragment transients at the same and slightly longer time delays. Characteristic examples of such power dependencies are shown in Figure 2; the slope is significantly larger than one and reflects a resonant two-photon excitation. These values are not integers because there is a certain overlay of a one-photon process and because saturation effects generally tend to reduce the slope.[11]

All the ketones under study, with the exception of 2,2,5,5-[D_4]cyclopentanone ([D_4]CP), were obtained from commercial sources and were used without further purification. [D_4]CP was prepared by H/D exchange of cyclopentanone in D_2O in 91% excess with respect to 2,2,5-[D_3]cyclopentanone. The purity was confirmed by a comparison

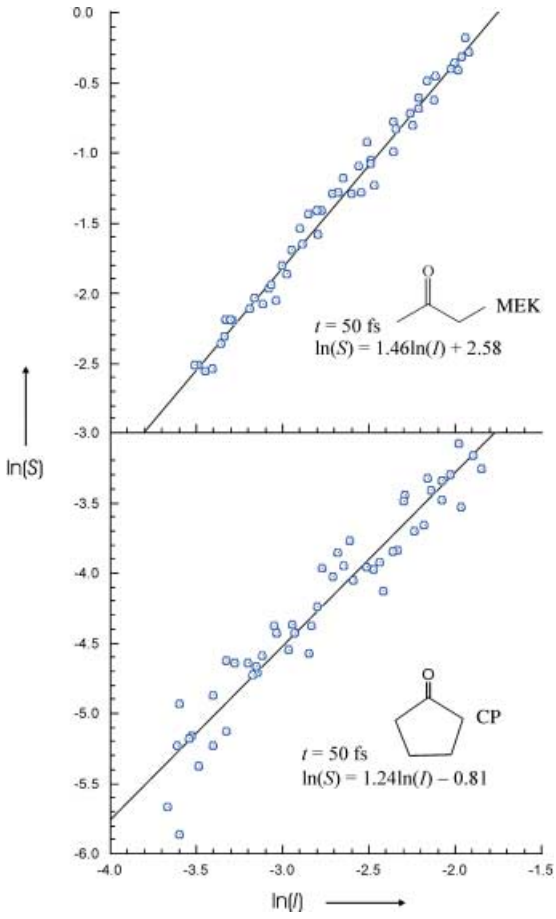

Figure 2. *Characteristic examples (MEK and CP) of power dependencies to show that two pump photons are involved in the excitation process.*

between the recorded mass spectra and those in the NIST data base.[23] The molecular beams were formed by expanding gaseous ketone seeded in helium from a total stagnation pressure of 20 psi. The pulse nozzle was heated to 130 °C in order to prevent clustering of molecules during the expansion.

Computational Methods

The necessary thermochemical quantities were obtained from ab initio molecular orbital calculations[24] performed with the Gaussian 98[25] suite of programs. The energies that relates to the S_2 species in Tables 2 and 3 are single-point calculations at the TD-B3LYP/6-31 + G(d) level, which has been shown to reproduce the six lowest transitions of the absorption spectrum of acetone quite well.[15] The geometries were optimized at the B3LYP/6-31 + G(d) level. This procedure gave results that are similar to those obtained under the CAS formalism.[16] The geometries of the ground-state molecules that are involved in this study and the corresponding relative energies were calculated at UB3LYP/6-31G(d) + ZPE (scaled as suggested by Scott and Radom).[26] Because of the size of some ketones under study we were limited to this level of computational sophistication. Using the barriers of the decomposition of the acyl radicals as a prototypical case, we verified that the relative energies obtained using the high-level G2(MP2) scheme[27] on the UB3LYP/6-31G(d) geometries show the same trends as found at the UB3LYP/6-31G(d) level. The transition-state geometries have in each case been validated by an intrinsic reaction coordinate analysis and by the calculation of vibrational frequencies (one imaginary frequency); for details see the preceding paper.[16]

2. Results and Analysis

2.1. Transients and the Elementary Steps

2.1.1. Prototypical Ketones

The transients obtained by measuring the temporal evolution of the parent and fragment ion currents that result from the probing process were in all cases fitted to the solution of the kinetic equations that arise from the model given in Equation (2); the equations are simply used to provide time constants but we must keep in mind characteristics of a coherent wave packet, for example bifurcation. The bifurcation for the decomposition of the A and B species is to be considered whenever the phase space involves direct and indirect trajectories, as discussed below. The solution to the kinetic equations can be found elsewhere,[28] and include the response function of the system.[29]

The branching of A shown in Equation (2) indicates the two channels possible for asymmetric ketones; A and B together represent a distinct species but as discussed below the wave packet can bifurcate to give different trajectories for each of

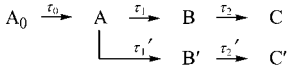

(2)

them. Previous studies did not resolve the initial step and the dynamic model employed did not include A_0.[2, 5, 6] The impetus for the incorporation of A_0 is best illustrated by two experimental results. Using xenon as a reference, the time where the intensity maximum of the pump and the probe pulses coincide (t_0) can be determined very accurately because the excited states of xenon have a negligible lifetime.[22, 30] In the case of MEK (Figure 3) such a calibration showed that the t_0 which is derived from the

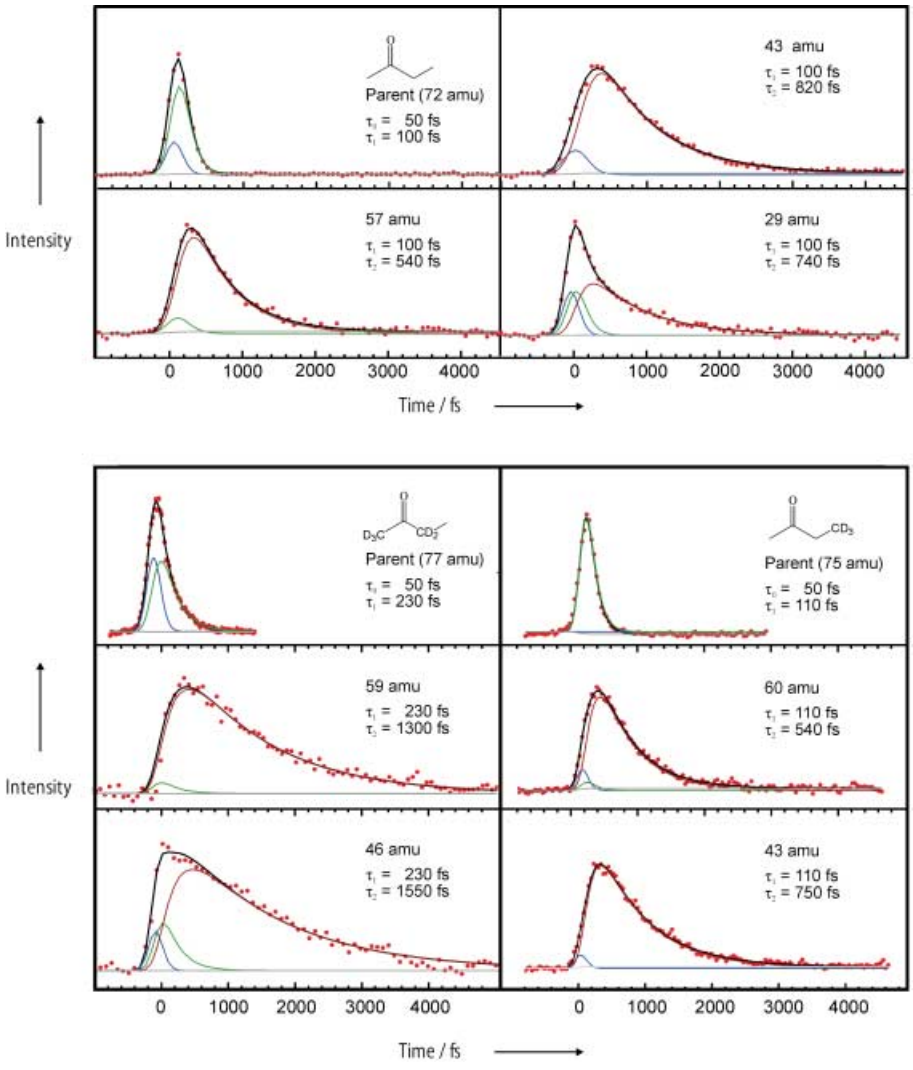

Figure 3. *Transients for the parent and fragment species that arise from MEK and its deuterated analogues. The experimental data points are given as red dots and the overall fit is shown as a black line. The various components of the transient are represented by different colors. The blue line corresponds to the initial 50 fs process; the green line represents the component with a 50 fs rise time and a decay time of τ_1; the red curve gives the component that rises with τ_1 and decays with τ_2. Note the pronounced influence of the α-deuterium substitution. The gray line is the nanosecond component that previously has been shown to correspond to a one-photon process.*[11]

fragment transients is shifted by approximately 50 fs relative to xenon. This indicates that an initial ultrafast component has to be included in order to obtain a fit which is consistent with the xenon calibration. Additionally, Figure 4 shows that the incorporation of this extra component was also necessary, particularly in the case of the transient taken at $m/z = 43$, in order to obtain a consistent set of fits (with respect to the xenon calibration and with respect to the fragment and parent transients) for DPK.

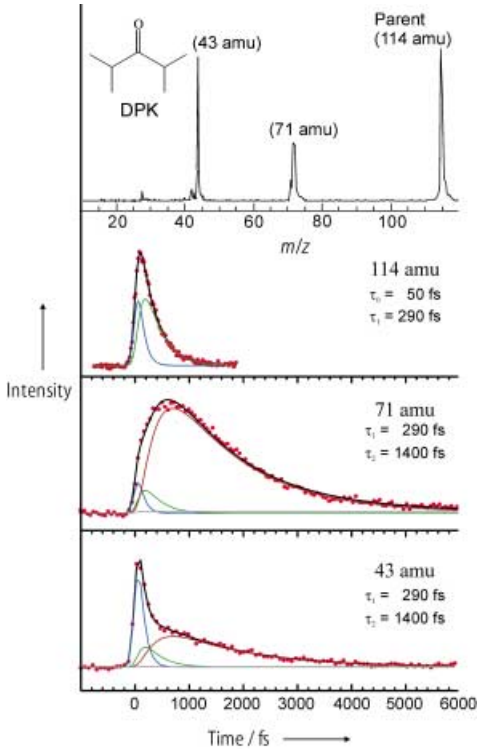

Figure 4. *Multiphoton ionization mass spectra of DPK at a time delay of less than 50 fs and the associated transients for the parent and fragment species. Color coding is the same as in Figure 3. Note the necessity of the initial 50 fs component for the transient taken at* m/z = *43.*

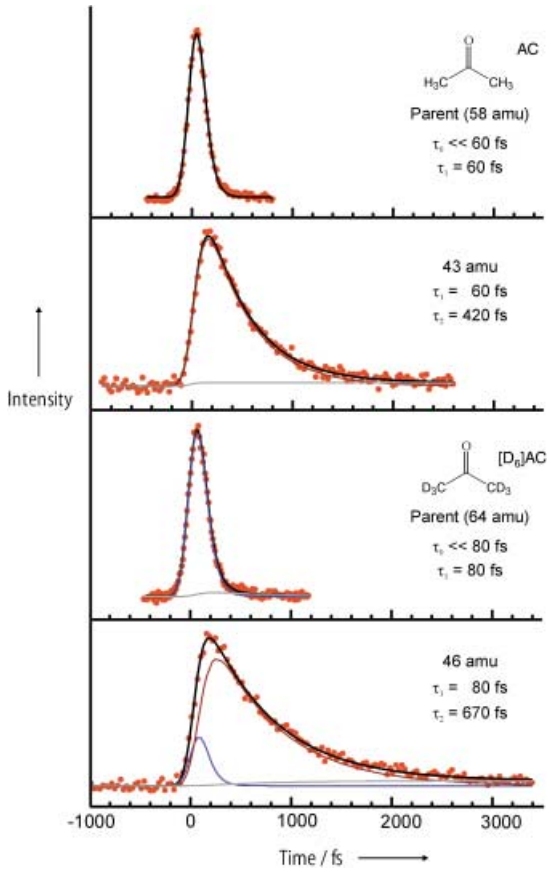

Figure 5. *Transients for the parent and fragment species from AC and [D_6]AC. The experimental data points are given as red dots and the overall fit is shown as a black line. In this case the component that corresponds to the internal conversion could not be resolved from the component that corresponds to the first bond breakage. The red curve gives the component of the second bond breakage and the difference in time scale between the deuterated and the undeuterated compound is evident. The gray line is the nanosecond component that previously has been shown to correspond to a one-photon process.*[11]

2.1.2. Other Ketones: τ_0, τ_1, and τ_2

The time constants that can be derived from the transients in Figures 3 – 9 are presented in Table 1. The initial ultrafast component is represented by a fixed 50 fs decay (τ_0) in all the investigated cases. Concurrently, the value for τ_1 was derived from the parent transient in question with t_0 and cross-correlation values fixed according to a preceding xenon calibration. The division of the parent transient into two components is evident throughout Figures 3 – 9; see for example the transient taken at the parent mass of MEK. The consistency with the xenon calibration was assured by a comparison of the values for t_0. The same procedure was employed for the fragment transients to obtain τ_2; in this case τ_0, τ_1, and the cross-correlation values were fixed according to the parent transient. The numbers in Table 1 will be discussed below as some trends are worth noticing. For example, with the notable exception of DBK, τ_1 increases with molecular size. The trend in the variation of τ_2 among the species in Table 1 is less obvious and it involves knowledge of energetics and kinetics as discussed later. For the cyclic ketones (Figure 8 and 9), the transients (in Figure 8) were taken using lower intensity of the probe pulse than for those in Figure 9, thus the initial spike-type component is much less pronounced for the transients in Figure 8.

2.2. Energetics for the Decomposition of Neutral and Ionic Species

Tables 2 – 5 present all the auxiliary thermochemical data that are required in analysis of the trends of the fs-resolved mass spectra, the time constants in Table 1, and ultimately the detailed mechanism for the Norrish type-I reaction. For some of the entries, experimental values are available,[23] but in order to be able to make internally consistent comparisons we have chosen to present calculated values throughout. When available, the experimental results agree with the calculated ones. The C–C bond breakage on the ground-state potential energy surface proceeds without an energy barrier; the reaction endothermic-

ities lie between 58.9 and 79.5 kcal mol^{-1} relative to the ground-state energy. The energetics for C—C bond breakage on the S_1 surface were presented in paper I of this series.[11] As opposed to the reactions on the ground-state surface, there is a saddle point involved when the bond breakage occurs from the S_1 state.[11] The barriers on the S_1 surface were found to follow the relative stability of the alkyl radical that is expelled, namely, they decrease in the order $CH_3^{\bullet} > C_2H_5^{\bullet} > iC_3H_7^{\bullet} > tC_4H_7^{\bullet}$. It is worth noting that isotope substitution hardly influences the barriers for the decomposition; an increase of only 1 kcal mol^{-1} upon α-deuterium substitution is found.[31] In the present study we also take reactions from the S_2 state into consideration. Because of the size of the systems under study and because of severe convergence problems of the third-root CAS wave function, the geometries of the stationary points that are associated with bond breakage on the S_2 surface are only calculated for acetone. A comparison of TDDFT potential energy surface scans and the energies obtained from the CAS optimization of the acetone transition state verifies that these two procedures give similar results. The barriers for C—C bond breakage on the S_1 and S_2 surfaces are comparable for acetone. TDDFT calculations have provided the reaction energies for the decomposition through a Norrish type-I reaction on the S_2 surface (Table 3), and the approximate barriers for the further decomposition of the acyl radicals that are formed upon the initial bond breakage on the S_2 surface (Table 4). For such a similar series of reactions, the reaction energies can be taken to reflect the corresponding energy barriers.

2.3. Femtosecond-Resolved Mass Spectra

Figure 10 shows the multiphoton ionization (MPI) mass spectra of acetone and [D_6]acetone. The mass spectra for the remaining ketones are shown in Figures 4, 11, and 12. They were recorded under conditions where the background (non time-dependant) signals were minimized. The time delay be-

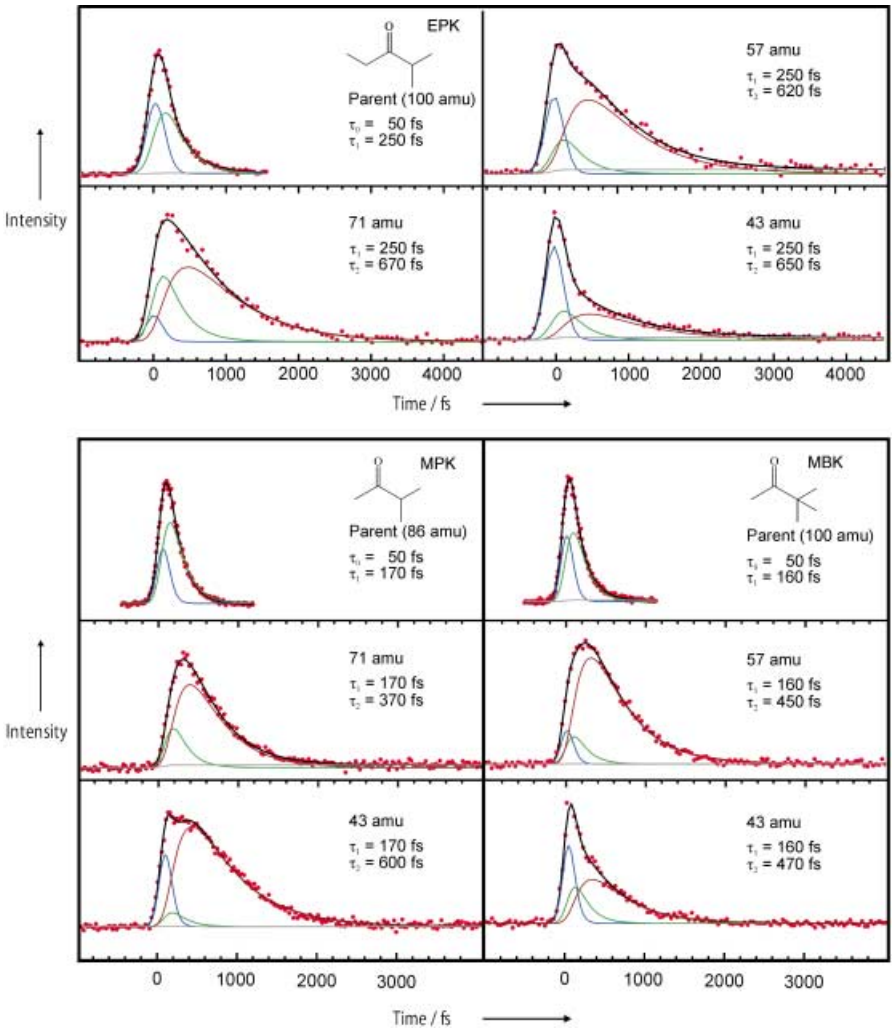

Figure 6. *Transients for the parent and fragment species that arise from asymmetric ketones EPK, MPK, and MBK. Color coding is the same as in Figure 3.*

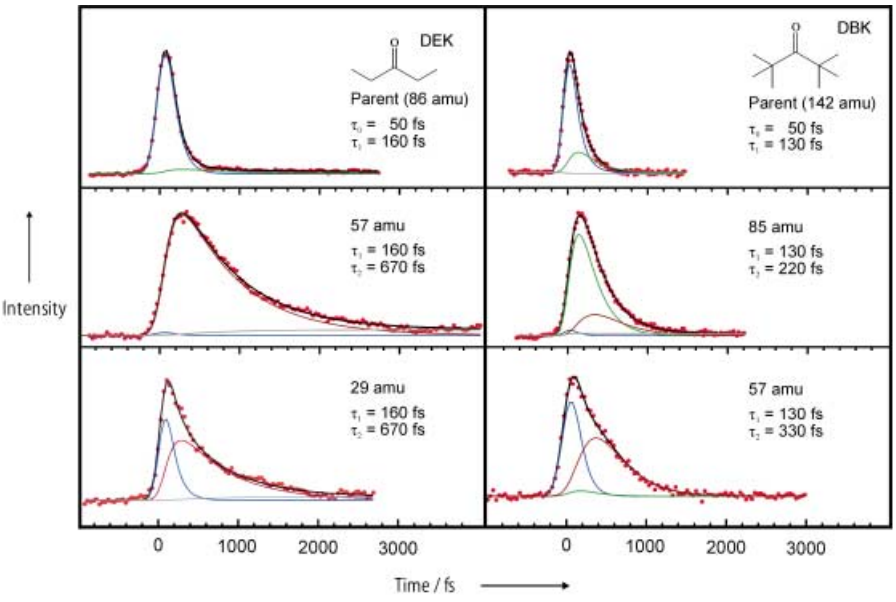

Figure 7. *Transients for the parent and fragment species that arise from symmetric ketones DEK and DBK. Color coding is the same as in Figure 3.*

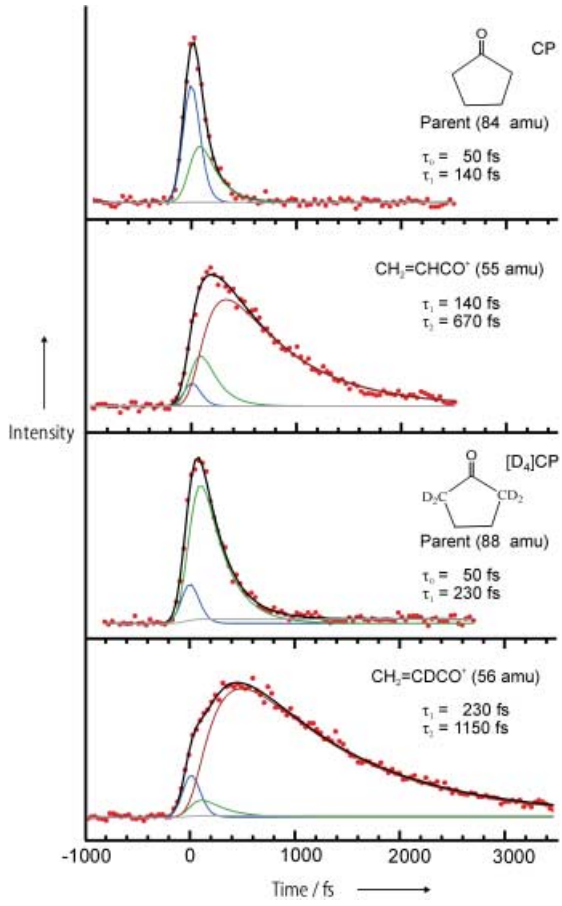

Figure 8. *Transients taken at the parent mass and at the mass that corresponds to the base peak in the mass spectra of CP and [D4]CP. Color coding is the same as in Figure 3. A very low intensity (~4 μJ) of the probe pulse was employed to reduce the contribution of the parent ion fragmentation to the transients taken at the fragment mass.*

tween the pump and probe pulses was chosen to be less than 50 fs. At this short time delay, no significant decomposition of the neutral parent molecule has taken place and the mass spectra therefore mainly reflect MPI-induced ionization and fragmentation of the parent species. A comparison with the literature[23] 70 eV electron-impact ionization (EI) mass spectra shows that these two ionization techniques give very similar results. This confirms the purity of the samples and the absence of residual samples in our molecular beam apparatus. The only difference between the MPI and the EI spectra is that the parent peak is higher than any of the fragment peaks in the MPI spectra. This difference shows that MPI ionization with the wavelength and intensity (~6 μJ) that we have employed is a softer ionization method, since it produces molecular ions that fragment less readily. The use of fs pulses ensures the selective ionization of the parent.

2.3.1. Ion Chemistry and Femtosecond-Resolved Mass Spectra

Since the mass spectra in Figures 4 and 10–12 have been recorded at a very short time delay between the pump and the probe pulses, no decomposition of the neutral parent species has yet occurred. These mass spectra therefore offer the prospect of a discussion on the fs pulse-induced ion chemistry of the parent species in question. The fragmentation pattern of the parent radical cations closely resembles that of the excited-state neutral molecules. The appearance of the mass spectra is influenced by the primary decomposition of the parent ion to form a set of fragment cations and by the secondary (and tertiary) decomposition reactions of these fragment ions.

Computational results show that the simple cleavage reactions of the ketone radical cations proceed without an energy barrier in addition to the reaction endothermicity (Table 2). The rationalization of the relative heights of the peaks that result from the decomposition of the asymmetric ketone radical cations is not in all cases consistent with the expectations that

Table 1. *Time constants related to the Norrish type-I reactions.*

Molecule	Probed Species		τ_0 [fs]	τ_1 [fs]	τ_2 [fs]
AC	Parent	($m/z=58$)		60	
	$CH_3C{\equiv}O^+$	($m/z=43$)		60	420
[D_6]AC	Parent	($m/z=58$)		80	
	$CD_3C{\equiv}O^+$	($m/z=46$)		80	670
MEK	Parent	($m/z=72$)	50	100	
	$CH_3CH_2C{\equiv}O^+$	($m/z=57$)	50	100	540
	$CH_3C{\equiv}O^+$	($m/z=43$)	50	100	820
	$CH_3CH_2^+$	($m/z=29$)	50	100	740
α-MEK	Parent	($m/z=77$)	50	230	
	$CH_3CD_2C{\equiv}O^+$	($m/z=59$)	50	230	1300
	$CD_3C{\equiv}O^+$	($m/z=46$)	50	230	1550
β-MEK	Parent	($m/z=75$)	50	110	
	$CD_3CH_2C{\equiv}O^+$	($m/z=60$)	50	110	540
	$CH_3C{\equiv}O^+$	($m/z=43$)	50	110	750
MPK	Parent	($m/z=86$)	50	170	
	$(CH_3)_2CHC{\equiv}O^+$	($m/z=71$)	50	170	370
	$CH_3C{\equiv}O^+$[a]	($m/z=43$)	50	170	600
MBK	Parent	($m/z=100$)	50	160	
	$(CH_3)_3CC{\equiv}O^+$	($m/z=85$)			
	$(CH_3)_3C^+$	($m/z=57$)	50	160	450
	$CH_3CHCH_3^+$[b]	($m/z=43$)	50	160	470
DEK	Parent	($m/z=86$)	50	160	
	$CH_3CH_2C{\equiv}O^+$	($m/z=57$)	50	160	670
	$CH_3CH_2^+$	($m/z=29$)	50	160	670
EPK	Parent	($m/z=100$)	50	250	
	$(CH_3)_2CHC{\equiv}O^+$	($m/z=71$)	50	250	670
	$CH_3CH_2C{\equiv}O^+$	($m/z=57$)	50	250	620
	$CH_3CHCH_3^+$	($m/z=43$)	50	250	650
DPK	Parent	($m/z=114$)	50	290	
	$(CH_3)_2CHC{\equiv}O^+$	($m/z=71$)	50	290	1400
	$CH_3CHCH_3^+$	($m/z=43$)	50	290	1400
DBK	Parent	($m/z=142$)	50	130	
	$(CH_3)_3CC{\equiv}O^+$	($m/z=85$)	50	130	220
	$(CH_3)_3C^+$	($m/z=57$)	50	130	330
CP	Parent	($m/z=84$)	50	140	
	$CH_2CH_2C{\equiv}O^{+\bullet}$	($m/z=56$)	50	140	660
	$CH_2{=}CHC{\equiv}O^+$	($m/z=55$)	50	140	670
	$CH_2C{\equiv}O^{+\bullet}$	($m/z=42$)	50	140	680
	$CH_2{=}CH{-}CH_2^+$	($m/z=41$)	50	140	680
[D_4]CP	Parent	($m/z=88$)	50	230	
	$CD_2CH_2CH_2CD_2^{+\bullet}$	($m/z=60$)	50	230	1150
	$CH_2{=}CDC{\equiv}O^+$	($m/z=58$)	50	230	1100
	$CH_2CD_2C{\equiv}O^{+\bullet}$	($m/z=56$)	50	230	1150
	$CD_2C{\equiv}O^{+\bullet}$	($m/z=44$)	50	230	1150
	$CD_2{=}CH{-}CH_2^+$	($m/z=43$)	50	230	1150

[a] Isobaric with $CH_3CH_2CH_2^+$, see text. [b] Isobaric with $CH_3C{\equiv}O^+$, see text.

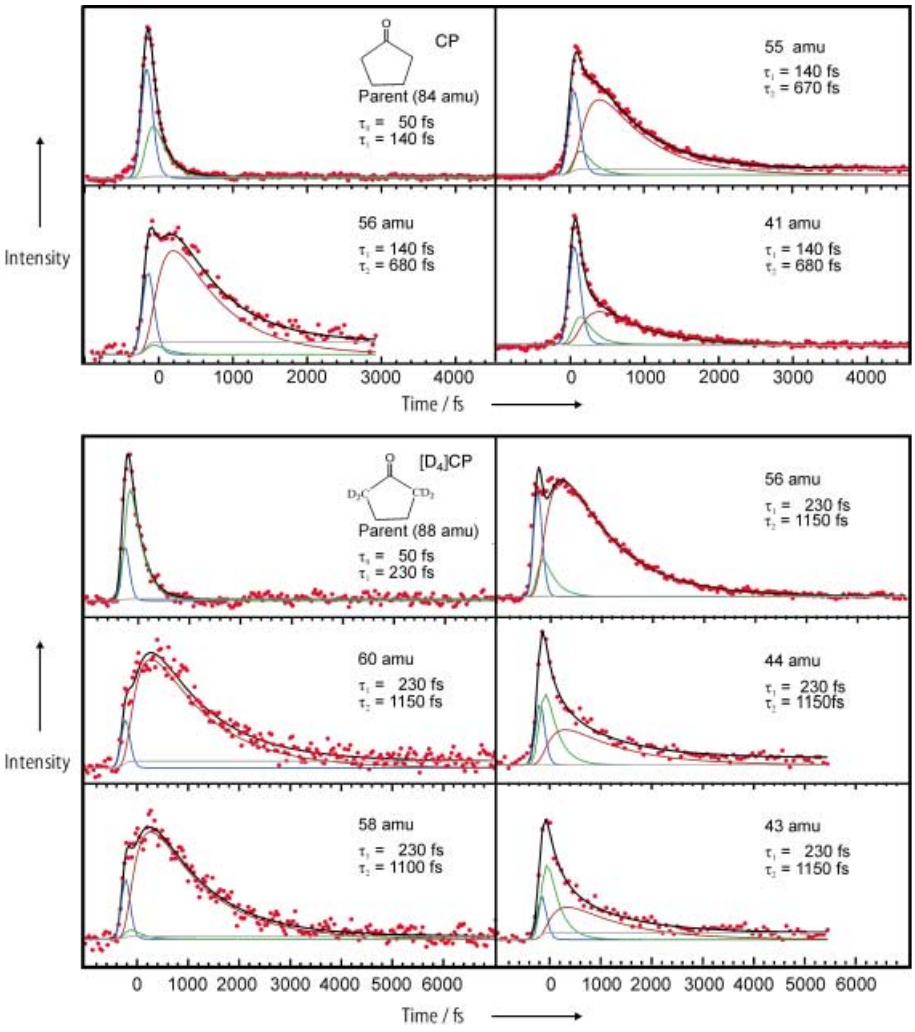

Figure 9. *Transients for the parent and fragment species of CP and [D_4]CP. Color coding is the same as in Figure 3. An intermediate intensity of the probe was used (~15 μJ) giving a reasonable signal-to-noise ratio for the less abundant species. Note the pronounced spike-like contribution from fragmentation of the parent ion.*

Table 2. *Reaction energies for the decomposition of the ionized ketones.*[a]

Molecule	R′-CO-R		−•R′		−•R	
	•R′	•R	ΔH_r •R′ + RCO$^+$	ΔH_r $^+$R′ + RCO•	ΔH_r R′CO$^+$ + R•	ΔH_r R′CO• + R$^+$
MEK•$^+$	CH_3	CH_2CH_3	1.12	4.11	1.24	2.36
α-MEK•$^+$	CH_3	CD_2CH_3	1.17	4.15	1.26	2.35
β-MEK•$^+$	CH_3	CH_2CD_3	1.12	4.11	1.24	2.35
MPK•$^+$	CH_3	$CH(CH_3)_2$	1.14	4.34	1.31	1.55
MBK•$^+$	CH_3	$C(CH_3)_3$	1.11	4.47	1.32	0.95
EPK•$^+$	CH_3CH_2	$CH(CH_3)_2$	1.18	2.73	1.24	1.70
AC•$^+$	CH_3	CH_3	1.15	3.92		
[D_6]AC•$^+$	CD_3	CD_3	1.20	3.96		
DEK•$^+$	CH_3CH_2	CH_2CH_3	1.19	2.54		
DPK•$^+$	$(CH_3)_2CH$	$CH(CH_3)_2$	1.21	1.87		
DBK•$^+$	$(CH_3)_3C$	$C(CH_3)_3$	0.79	1.01		

[a] Enthalpy at 0 K at B3LYP/6-31G(d) level; values in eV ($\Delta H = \Delta U + \Delta pV$, where U is the potential energy and $\Delta pV = \Delta nRT = 0$ at 0 K; see ref. [58]).

can be formed from the energetics for the primary decomposition of the parent radical cations. In the following the reason for this is discussed.

The mass spectrum of MEK only shows very small peaks at the masses corresponding to the alkyl cations (CH_3^+ and $C_2H_5^+$). Thus, the discussion of the decomposition of MEK is not complicated by secondary fragmentation. From the mass spectrum of MEK it can be seen that the formation of the acetyl cation (loss of an ethyl radical from MEK•$^+$) proceeds in the highest yield, regardless that the energy demand for this reaction is higher than the energy demand for the formation of a propionyl cation (methyl loss from MEK•$^+$; see Table 2). This phenomenon is well known from the decomposition in the ion source of radical cations that have been formed by electron-impact ionization.[32–34] The observation, however, is new to a "true" microcanonical ensemble. The result for the yield in such competing simple cleavages has been found to be due to an interplay between the barrier heights of the two competing reactions and the position of the transition states for the simple cleavage reactions.[35, 36] The transition states for the more energy demanding of the two (otherwise similar) competing reactions has been shown to be more loose.[35, 37] When sufficient internal energy is available, the energetic advantage becomes insignificant compared to the smaller spacing between the vibrational levels in transition state for more energy-demanding reaction (the looser transition state). The internal energy at which the more energy-demanding reaction takes over is obviously determined by how different the demands for the two competing simple cleavage reactions are. The energetically favored reaction *will* dominate if the available excess energy is small compared to the difference between the critical energy for the two competing simple cleavages.

The mass spectrum of MPK shows that the peak corresponding to loss of an isopropyl radical ($m/z = 43$) is significantly higher than the peak that corresponds to the loss of a methyl radical ($m/z = 71$), although the reaction energy for loss of the methyl radical is 4 kcal mol^{-1} lower than the reaction energy for loss of an isopropyl radical (Table 2). Again, regardless of the energetic preference for the loss of the smaller fragment, the larger alkyl radical is lost in the higher yield. The associated transient show that the peak at $m/z = 43$ does have a substantial contribution from the propyl cation because it more closely resembles the transients taken at the mass of an alkyl cation than

Table 3. *Reaction energies for Norrish type-I reaction on the S_2 surface.*[a]

Molecule	R′-CO-R			−•R′		−•R	
	•R′	•R	$E(S_2)$	ΔH_r •R′ + 3s-RCO•	ΔH_r 3s-•R′ + RCO•	ΔH_r 3s-R′CO• + R•	ΔH_r R′CO• + 3s-R•
MEK	CH_3	CH_2CH_3	6.14	0.32	3.08	0.43	1.76
MPK	CH_3	$CH(CH_3)_2$	5.99	0.51	3.17	0.43	1.31
MBK	CH_3	$C(CH_3)_3$	5.98	0.44	3.10	0.18	0.72
EPK	CH_3CH_2	$CH(CH_3)_2$	5.97	0.31	1.79	0.11	1.25
AC	CH_3	CH_3	6.17	0.55	3.05		
DEK	CH_3CH_2	CH_2CH_3	6.08	0.24	1.82		
DPK	$(CH_3)_2CH$	$CH(CH_3)_2$	5.85	0.35	1.39		
DBK	$(CH_3)_3C$	$C(CH_3)_3$	5.89	−0.29	0.40		

[a] 0 K TD-B3LYP/6-31 + G(d) values in eV for the decomposition of R′(C=O)R to form an acyl and an alkyl radical.

Table 4. *Vertical and adiabatic ionization energies of the 3s acyl radicals and the barriers and reaction energies for their decomposition.*[a]

Reaction	E(3s)	$\Delta H^{\neq}$	ΔH_r	Vertical IE[b]
$CH_3C{=}O^{\bullet} \rightarrow CH_3^{\bullet} + C{=}O$	3.09	0.13	−2.54	4.1
$CH_3CH_2C{=}O^{\bullet} \rightarrow CH_3CH_2^{\bullet} + C{=}O$	2.83	0.08	−2.37	4.1
$(CH_3)_2CHC{=}O^{\bullet} \rightarrow (CH_3)_2CH^{\bullet} + C{=}O$	2.93	0.01	−2.60	3.9
$(CH_3)_3CC{=}O^{\bullet} \rightarrow (CH_3)_3C^{\bullet} + C{=}O$	2.93	0.00	−2.71	3.7

[a] 0 K TD-B3LYP/6-31 + G(d) values in eV. [b] For technical reasons the values correspond to single-point calculation on the geometry of the cation, thus, the calculated adiabatic ionization energies are equal to the vertical ionization energies.

Table 5. *Vertical and adiabatic ionization energies (IE) of the ground-state acyl radicals and the barriers and reaction energies for their decomposition.*[a]

Reaction	$\Delta H^{\neq}$	ΔH_r	Vertical IE	Adiabatic IE
$CH_3C{=}O^{\bullet} \rightarrow CH_3^{\bullet} + C{=}O$	0.65	0.55	8.5	7.0
$CH_3CH_2C{=}O^{\bullet} \rightarrow CH_3CH_2^{\bullet} + C{=}O$	0.54	0.46	8.3	6.8
$(CH_3)_2CHC{=}O^{\bullet} \rightarrow (CH_3)_2CH^{\bullet} + C{=}O$	0.43	0.33	8.0	6.6
$(CH_3)_3CC{=}O^{\bullet} \rightarrow (CH_3)_3C^{\bullet} + C{=}O$	0.32	0.22	7.8	6.4

[a] 0 K B3LYP/6-31G(d) values in eV.

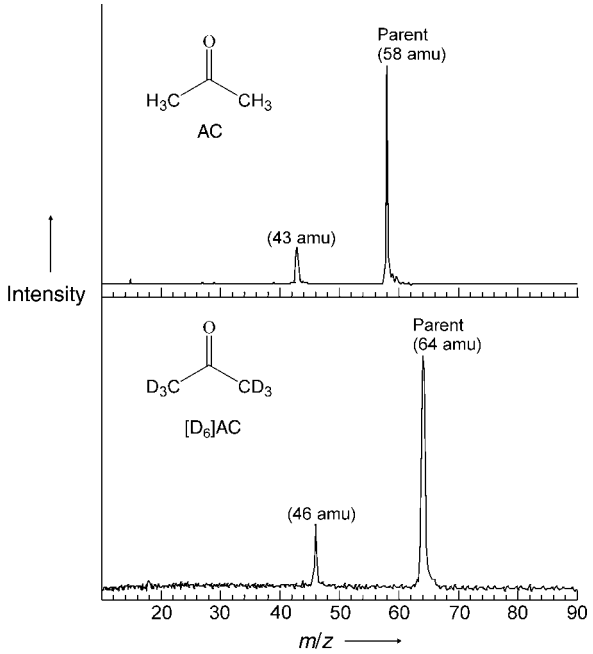

Figure 10. *MPI mass spectra of AC and [D_6]AC recorded at a time delay of less than 50 fs between the pump and the probe pulse.*

those taken at the mass of an acyl cation (compare the transient taken at $m/z = 43$ from MPK with the transients for EPK taken at $m/z = 43$ and 57, respectively; Figure 6). It is therefore possible, but not overly likely, that the effect is not in play here because the reaction energies differ more than in the case of MEK.

For MBK the difference for the energy demand for the two competing simple cleavages is 9 kcal mol^{-1} with the preferred reaction being the formation of a positively charged alkyl fragment and a neutral acetyl radical; this product ion ($m/z = 57$) does in fact give rise to the highest spectral peak. The reason why the alkyl fragment obtains the positive charge is related to the stability of the *tert*-butyl cation. The relation between cation stability and which fragment is to obtain the positive charge has been referred to as Stevenson's rule.[38]

The reaction energies for the two competing simple cleavages in EPK are very similar and it is difficult to judge whether the size effect is in play. The mass spectrum of EPK shows pronounced secondary fragmentation of the acyl cations (the formation of ethyl and isopropyl cations ($m/z = 29$ and 43) directly from the parent species have barriers that are much too high for the reactions to be competitive, Table 2). If the alkyl peak is superimposed with the peak for its precursor acyl cation ($m/z = 29$ plus $m/z = 57$, and $m/z = 43$ plus $m/z = 71$) the competing alkyl-loss reactions will seem to proceed in a comparable yield.

The decomposition of the ionized cyclic ketones is slightly more complicated (Figure 12). The initiating step is the formation of so-called distonic ion (an ion with separated charge and radical sites, the only neutral precursor of this species is a diradical)[39] and its further decomposition has been shown in several theoretical and experimental investigations to proceed as shown in Scheme 1.[38, 40, 41] The results for the deuterium-labeled species allow an assessment of the branching between the two species with a mass of 56 amu. In the case of the oxygen-containing species, the peak will be shifted to $m/z = 58$ whereas the hydrocarbon will appear at $m/z = 60$. The peak at $m/z = 58$ dominates. The mass spectrum of [D_4]CP also shows that the base peak at $m/z = 55$ in the mass spectrum of [D_0]CP does not

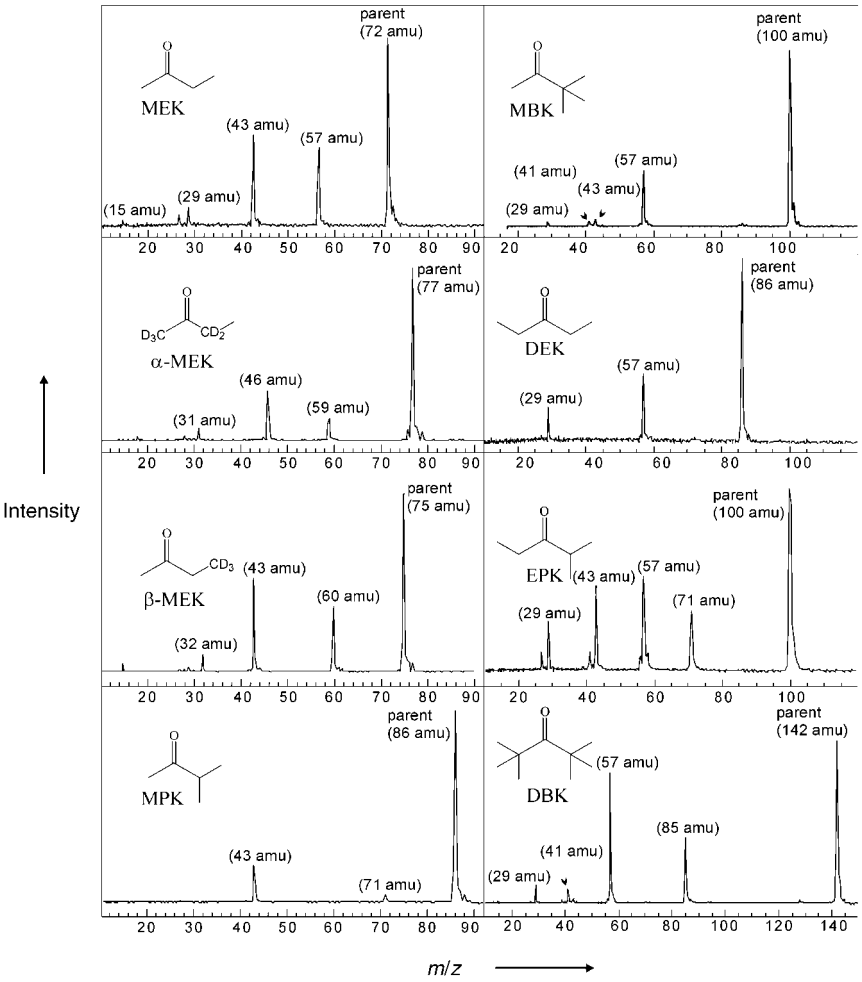

Figure 11. *Multiphoton ionization mass spectra of acyclic ketones recorded at a time delay of less than 50 fs between the pump and the probe pulse.*

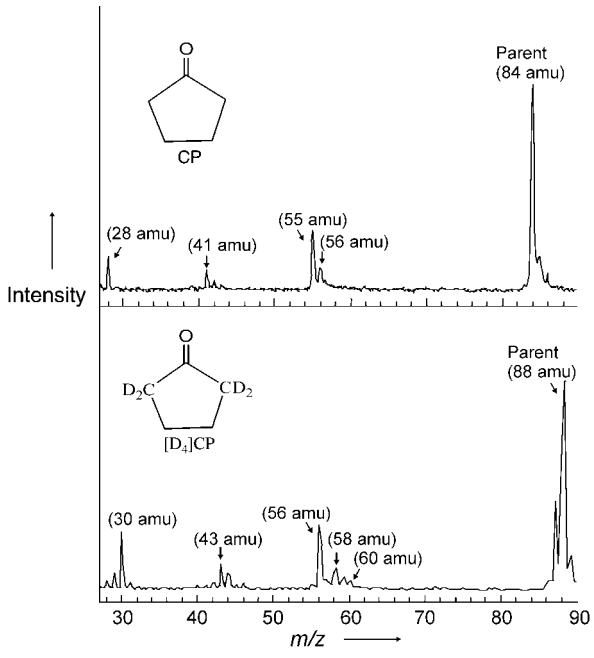

Figure 12. *Multiphoton ionization mass spectra of CP and $[D_4]$CP recorded at a time delay of less than 50 fs.*

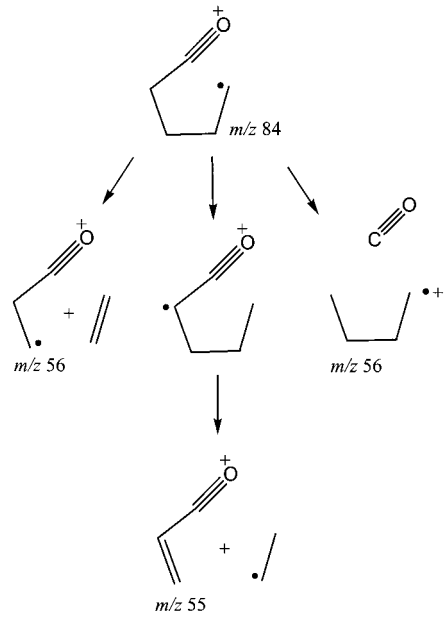

Scheme 1. *Mechanism for the decomposition of $CP^{\bullet+}$.*

result from the decomposition of the $m/z = 56$ carbocation by loss of a hydrogen atom; this might have been a viable pathway because it could eventually result in the formation of a very stable allylic carbocation. However, if that was the case the base peak in the mass spectrum of $[D_4]$CP would not have been found not four mass units away from the peak that corresponds to the carbocation but only one or two (loss of H or D from the carbocation). The mechanism for the decomposition of the deuterated distonic ion is shown in Scheme 2.

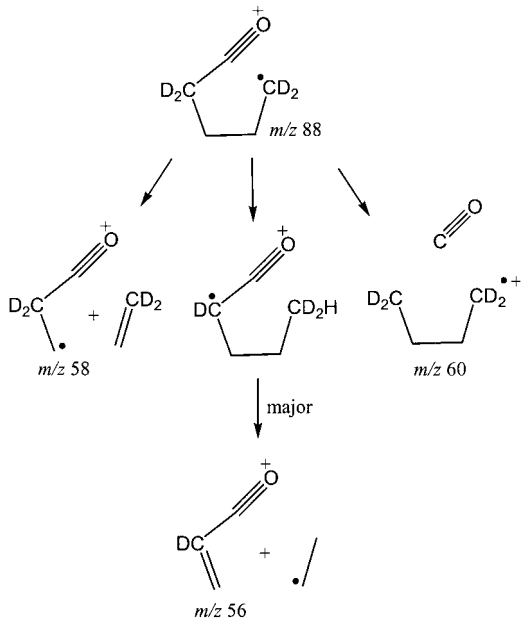

Scheme 2. *Mechanism for the decomposition of $[D_4]CP^{\bullet+}$.*

3. Discussion

3.1. Potential Energy Surfaces

3.1.1. A Prototypical Example

In the preceding paper of this series, we gave a detailed account of the computational investigation of the high-lying singlet states of acetone as a prototypical example of ketones.[16] In this paper we use the key results to draw the general dynamic picture of the underlying physical principles of the Norrish type-I reaction. The main impetus for the computational study was the search for a repulsive electronic state along the C–C coordinate. The characterization of such a state would unequivocally support the assignment of the initial ultrafast component in the acetone parent transient to the first bond breakage. However, a surface which is repulsive in the strict meaning of the word (σ* type) could not be found by us, neither with time-dependent density functional theory nor with sophisticated complete active space methods.

The calculations show that the initial ultrafast processes are governed by the C=O stretching motion. The energy for this motion is typically around 1750 cm^{-1} (~19 fs).[23] The cross-section of the potential energy surface along the C=O coordinate is shown in Figure 13. A detailed discussion of the surface

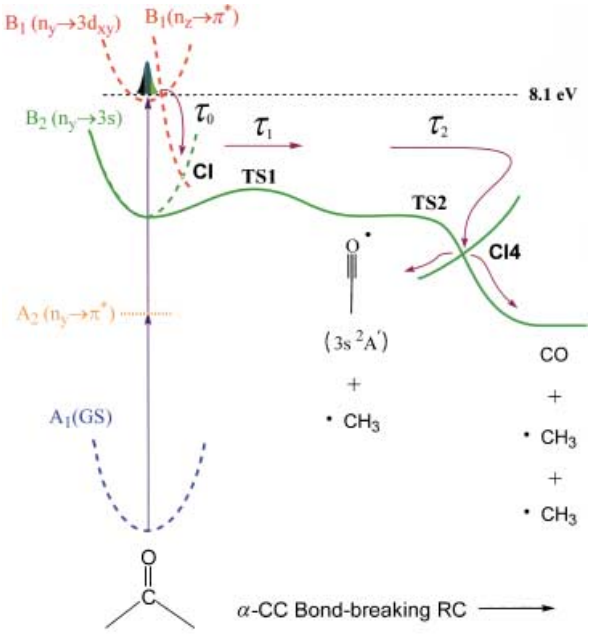

Figure 13. The dynamic picture representing the time scales for acetone along the α-CC bond-breaking RC, in a stepwise bond-dissociation mechanism, upon two-photon excitation at 8.1 eV (see text).

characterization is given in the preceding paper.[16] The energetics that are important for the purpose of the present paper are shown in Tables 3 – 5. The entire volume of computational and experimental results represent a validation and refinement of the schematic potential energy surface that was presented in our initial communication of the observation of the Norrish type-I reaction in real time.[2] The main feature to be noticed about the potential energy surface is simply that the Rydberg states are connected to the S_2(n,3s) state through a valence state via conical intersections (**CI**s) and that CC bond breakage is possible on the S_2 surface with a barrier of ~0.7 eV relative to the S_2 equilibrium species. The wave packet could, in principle, proceed even further to reach the S_1(n,π*) state also through a conical intersection (**CI1**), however, our calculations show that the energy of **CI1** is higher than that of **CI2** and that it becomes higher than 8.0 eV if the CCO out-of-plane bending motion is taken into account (the S_2 species is destabilized whereas the S_1 species is stabilized).[16] This result speaks against that internal conversion should proceed through to S_1. Additionally, the nature of **CI2** guides the wave packet towards a bond-breaking trajectory and diminishes the probability of further internal conversion from S_2. The nonadiabatic coupling vector associated with **CI2** is shown for acetone in Figure 14 and it can be seen that an asymmetric CC stretching motion dominates.

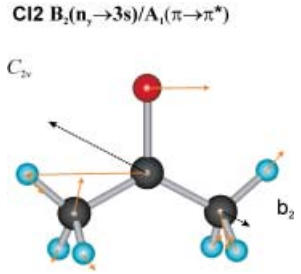

*Figure 14. Nonadiabatic coupling vectors of **CI2** showing the importance of the asymmetric C–C stretching motion that gives rise to the nonstatistical nature of the Norrish type-I reaction. The dotted lines show the projection of the forces along the C–C bond-breaking coordinate.*

The reaction coordinate for the bond breakage on the S_2 surface (Figure 15) is a combination of a CO in-plane bending motion and a CC stretching motion. The excited-state acyl radical formed from the bond-breaking reaction on the S_2 surface is linear and the CCO angle in the TS for the first bond breakage is therefore significantly distorted from the ~120° sp^2 bond angle in the acetone molecule. The excited-state acetyl radical further decomposes through a very small barrier (0.1 eV); this linear acetyl species is connected to the bent ground-state species via a conical intersection in one dimension whereas the CC bond stretches further in another. It is noteworthy that in this region the 3s acetyl PES has a substantial σ* character. This results in a surface which is effectively repulsive in nature. Some trajectories cross the transition state for the first bond breakage with nuclear arrangements that are very far from being linear, whereas some are very close to a linear configuration. Given the effective repulsive nature of the surface, the latter would give rise to very fast trajectories. However, this would not necessarily be the case for the nonlinear species.

3.1.2. Relation to Previous Results

A conical intersection is conventionally considered to offer the possibility of a very efficient electronic transition from one

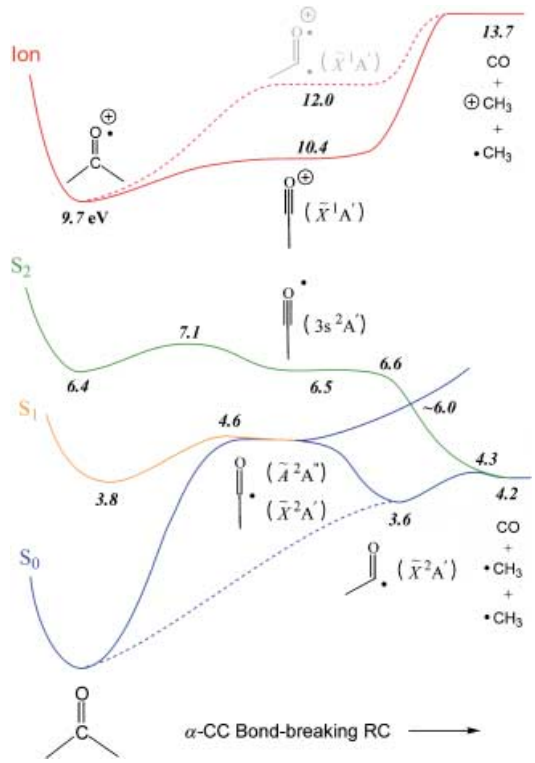

Figure 15. *Potential energy profiles along the C–C bond-breaking coordinate derived from the present work showing the ground-state surface and reaction path along the first two excited singlet states of neutral acetone. All solid curves represent the path for a linear acetyl radical while the dotted curves represent the path for the bent acetyl radical. The C–C bond breakage is also shown for the ground state of the radical cation, to indicate the changes in ionization potential along the reaction coordinate. The indicated numbers are the energy values [eV] above the ground state, obtained from the theoretical calculations in paper III.*[16]

surface to another.[42] It is therefore possible that the wave packet will arrive at the S_2 state after approximately half a C=O vibrational period, namely in 10 fs. This lower limit can only be reached if the very first visit to the conical intersection region of the potential energy surface is successful. Not only do the conical intersections efficiently take the wave packet from the highly excited states to the S_2 state, they also direct the energy that is being partitioned during the internal conversion process into an exclusive subset of the molecular degrees of freedom. In this manner, they guide a very fast nonconcerted C–C bond breakage. This picture is consistent with the nonstatistical behavior of the photochemically induced reactions.[20] Such an ultrafast internal conversion is in line with the broad (predissociative around the 0-0 band) absorption spectrum of acetone found by Vaida's group[43, 44] and the very broad absorption at higher energies for ketones.[19] A very broad spectrum reflects an ultrashort decay time, which typically is not characteristic of purely (bound) Rydberg states.

The groups of Lee and Houston have studied the translational energy that accompanies the decomposition of the acetyl radical from a variety of precursors.[17] The results[17b] from the excitations above the barrier on S_1, but below the barrier for CC cleavage on the S_2 surface, indicate that there is a barrier for the decomposition of the intermediate acetyl radical; the results in ref. [17d] suggested a concerted pathway (using the rotational clock criterion) while those in ref. [17b] suggested a more nonconcerted one. Our earlier real-time results[2, 5, 6] and those reported here indicate the nonconcerted nature of the reaction. The potential energy surface that we present in Figures 13 and 15 is entirely consistent with real-time results and with those of energy disposal.

3.1.3. Observables in Femtosecond-Resolved Mass Spectrometry

In the light of the results of the fs-resolved mass spectrometry experiments that were outlined in the previous Section, we further address the dynamic aspects of the Norrish type-I reaction for a broader range of molecules. Our detection window depends on the ionization cross-section. In connection with the acetyl radical it is worth noticing that our experiment is particularly sensitive for probing the excited-state species because the vertical ionization potential is favorable, in this case, over the bent state. The main reason for this is that the geometry of the Rydberg-state acetyl radical is very similar to the geometry of the acetyl cation and that the potentials for the two species, therefore, changes similarly by nuclear distortions, such as a CCO inplane bending, as shown in Figure 15 and 16. The barriers for the decomposition of the excited-state acetyl radicals that are relevant to our investigation are presented in Table 4 together with the vertical and adiabatic ionization potentials. We have considered the possibility of a bifurcation between the excited-state acetyl radical and the excited-state alkyl radical upon the first bond breakage (Figure 17). For energetic reasons it

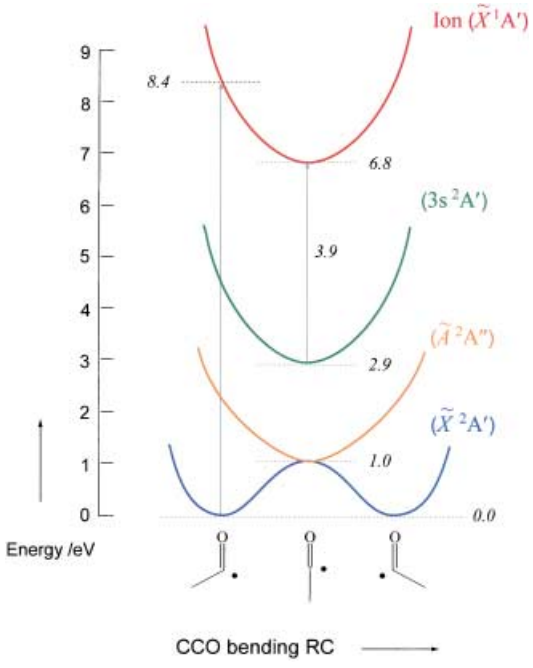

Figure 16. *The change in ionization potential with the CCO bending angle. Note the preference for ionization of the linear acetyl radical, and the independence of the ionization potential on the CCO motion for the linear (excited) radical but not for the bent (ground-state) radical.*

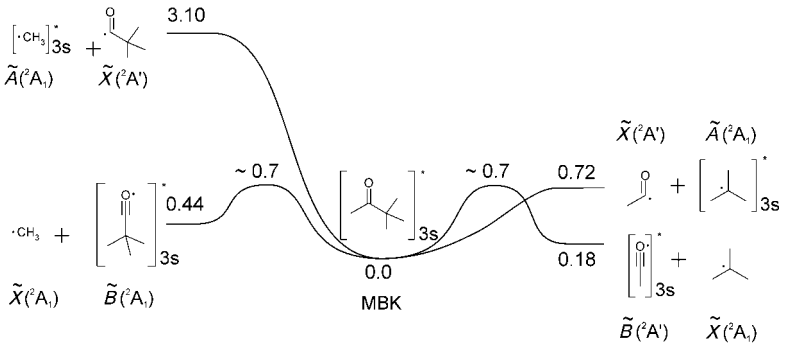

Figure 17. Schematic presentation of the potential energy profile along the coordinate for breakage of the first CC bond in MBK on the S_2 surface illustrating the possibility of branching between 3s alkyl and 3s acyl products. The numbers shown are relative energies [eV] with respect to 3s MBK.

would seem that it is only likely to occur in the case of MBK. For comparison, we also include the corresponding ground-state values (Table 5). The importance of these findings are discussed in relation to the experimental results in the following Sections.

3.2. Time Scales: τ_0, τ_1, and τ_2

3.2.1. The Initial Internal Conversion through Conical Intersections (τ_0)

The first row of time constants in Table 1 (τ_0), which in the above picture describes processes that take the wave packet out of the Franck–Condon region and down to the S_2 state via the C=O stretching mode and two conical intersections. We note that the only cases where the τ_0 component could be resolved with absolute certainty were those of MEK and DPK. Thus, the magnitude of τ_0 might vary slightly, although the passing of a conical intersection is normally very efficient. In contrast, a Fermi golden-rule type internal conversion, which is conditioned by the density of states, would take several picoseconds. In fact, this passing of a conical intersection is quite common on the femtosecond timescale (see for example refs. [22, 42, 45]). Since the C=O stretch occurs in 20 fs, our derived value of 50 fs or less is consistent with the time scale of the motion toward the intersection and with the initial lifetime broadening of spectra (see ref. [19] and references therein).

3.2.2. The First Bond Breakage (τ_1)

As prescribed by Equation (2), the second column of Table 1 gives the reaction time (τ_1) for the first CC bond breakage. The reaction path that is being followed is described by the stretching of the CC bond and the concurrent CCO inplane bending to form an acetyl radical. This conclusion about τ_1 is in line with the results of previous real-time studies,[2–12] and we are now able to provide the details regarding the electronic structure of the acyl radical that is being formed in the process.

The time constant for the first bond breakage (τ_1 values in Table 1) somewhat increases (with the single exception of DBK) as the molecular size increases. In most cases the energy barrier decreases as the molecular size increases. If the energy barrier was solely involved in the determination of the rate, this would have resulted in a larger rate for bond breakage as the molecular size increases. Accordingly, the change is due to the motion of the wave packet in the reduced space, made of the subset of the activated degrees of freedom, which increases with molecular size. Clearly the impact of the molecular size is nowhere near as significant as anticipated from an RRKM consideration, thus the nonstatistical behavior of the first bond breakage, as discussed below. The results in Table 3 shows that the decomposition of DBK is the only reaction which is exothermic and it also shows that the reaction has the lowest energy requirement for the formation of a Rydberg-state alkyl radical. In fact, there are several indications in the direction that the behavior of DBK is different from the reminder of ketones under study; see the discussion below.

The time constant corresponding to the first bond breakage in cyclopentanone in Table 1 indicates that the Norrish type-I reaction in cyclic ketones proceeds in the same manner as in acyclic ketones; the first bond breakage takes 140 fs which is similar to the time it takes for the CC bond to break in the acyclic C_5 ketones. The most notable difference between the cyclic and the acyclic ketones is that in the cyclic case an acyl–alkyl diradical ($^{\bullet}CH_2CH_2CH_2CH_2C{=}O^{\bullet}$) is formed as an intermediate subsequent to the first bond breakage.

From Table 1 it can be seen that significant isotope effects are involved upon α-deuterium substitution whereas β-substitution does not influence the time constants—very much in line with the fact that a chemical bond is being broken. Computationally we have found that the energy barrier for the first bond breakage increases by less than one kcal mol^{-1} upon α-substitution and that it is unchanged upon β-substitution.[31] This small change can hardly be expected to cause the large effects that are in play for α-MEK in the case of the first bond breakage. Accordingly, the isotope effect is attributed to the involvement of the umbrella motion that is involved in the bond-breaking reaction, taking the α-carbon from its original sp^3 configuration to its planar sp^2 configuration in the alkyl radical. This process slows down significantly upon α-deuterium substitution. In the organic chemistry literature, this α-isotope effect is known and attributed to an involvement in the reaction coordinate.

3.2.3. The Second Bond Breakage (τ_2)

The time constants (τ_2) obtained from the transients recorded at fragment masses describe the decomposition of the product acyl radicals, as suggested previously.[2–12] Thus, the temporal evolution of the fragment ions maps how the population of the corresponding neutral fragments evolves in time; the fragment ions are formed by ionization of the corresponding neutral species and only to a minor extent by decomposition of the parent ion. This feature is unique to femtochemistry as one is able to observe the evolution from the parent to the fragment.

For the cyclic ketones, the acyl–alkyl diradical is ionized directly. The ionization results in decomposition, and the decay time of the acyl–alkyl diradical to form a tetramethylene diradical is therefore monitored in the fragment ions. The similarity of this scenario to what we have reported previously for the Norrish type-II reaction is noteworthy.[46] In that case the fragments from the decomposition of a similar ionized diradical ($H_3C\overset{+}{C}(OH)CH_2CH_2C^{\bullet}HR$) also reflects the decomposition of the neutral diradical. A theoretical investigation has shown that the cyclopentanone radical cation lies 14.7 kcal mol^{-1} lower in energy than the distonic ion, and that the barrier for the further decomposition of the distonic ion is close to 28 kcal mol^{-1}.[40] At a first glance it may seem inconsistent that ring closure is not an efficient pathway and that the slow τ_2 component therefore does not appear in the transients that are recorded at the parent mass. However, when sufficient energy is available, the decomposition will, for reasons of entropy, result in an increase in the number of molecules. Additionally, we note that for the intramolecular ring opening of neutral cyclopentanone no energy is released in the bond breakage. The internal energy is carried over to the ion upon ionization resulting in the formation of a highly (vibrationally) excited distonic ion.

As was the case for the first bond breakage, there is also a significant isotope effect in play for the second bond breakage. In this case the energy barrier is small (Table 3) and a small change could have a large influence. Entropy effects are usually important when the species in question resides in a shallow minimum. Trajectories which leave the phase space of the acetyl radical are therefore influenced by deuterium substitution. Thus in this case, as was also the case for τ_1, it is most likely that the umbrella motion is responsible for the isotope effect.

The experimental data elucidates the geometry of the acyl radical and its decay by τ_2; the key issue is the change in ionization potential. When the bond breakage occurs on the S_2 surface the product acyl radical is linear. The corresponding cation also is linear; the vertical ionization potential of the linear acyl radical is 4.5 eV lower than that of the bent ground-state geometry (Figure 16). Thus, it is much more likely to ionize the linear over the bent structure. Moreover, there are some indications that ground-state bent acyl radical is dark under our experimental conditions. Experiments on acetyl chloride may support this point. For acetyl chloride the presence of a state which is repulsive in the C—Cl coordinate is well established,[47] and we have performed TDDFT calculations to verify the existence of a repulsive surface in the vicinity of 8 eV that correlates with the (bent) ground state of the acetyl radical. The calculations were not absolutely conclusive because of strong interaction with the 3s Rydberg state.

However, the experimental transients recorded at the mass of the acetyl and [D_3]acetyl radicals from acetyl chloride (Figure 18) give time constants which are similar in magnitude to each other and to those that correspond to the first bond breakage in all the other cases ($\tau_0 \sim 50$ fs and $\tau_1 \sim 100$ fs). These results indicate that the acetyl cation is formed only by decomposition of the acetyl chloride radical cation, suggesting that the bent ground-state acetyl radical is not ionized under the stated experimental conditions. It is noteworthy that the energy partitioning among the fragments from the decomposition of acetyl chloride disfavors the chlorine atom (at least if an impulsive model is assumed) and thus leaves more energy in the acetyl radical, in comparison with all ketones under study here.

The results for the time constants in Table 1 are in line with the proposed mechanism for bond breakage. The time it takes for the C—C bond to break is influenced by an interplay between the available rotational, vibrational, and conformational degrees of freedom (entropy) and the barrier height of the reaction (energetics). These factors often work in opposite directions and therefore the trends of the time constants in Table 1 are not indicative of one particular change. The dynamic interpretation of the τ_2 values is discussed in Section 4.

There are some clear-cut predictions to be made from this mechanism with regard to the transients that correspond to alkyl fragment ions, namely that the transients for the alkyl fragment ions that are formed upon secondary fragmentation of the acyl cations will give rise to the same time constant as the transient for the precursor acyl cation, as exemplified for the fragments of EPK (the isobutanoyl and propionyl radicals) in Equation (3). Within experimental error, this is indeed the case for MEK and EPK (see Table 1). Note that direct ionization of the alkyl radicals would result in a signal that initially rises as a function of time

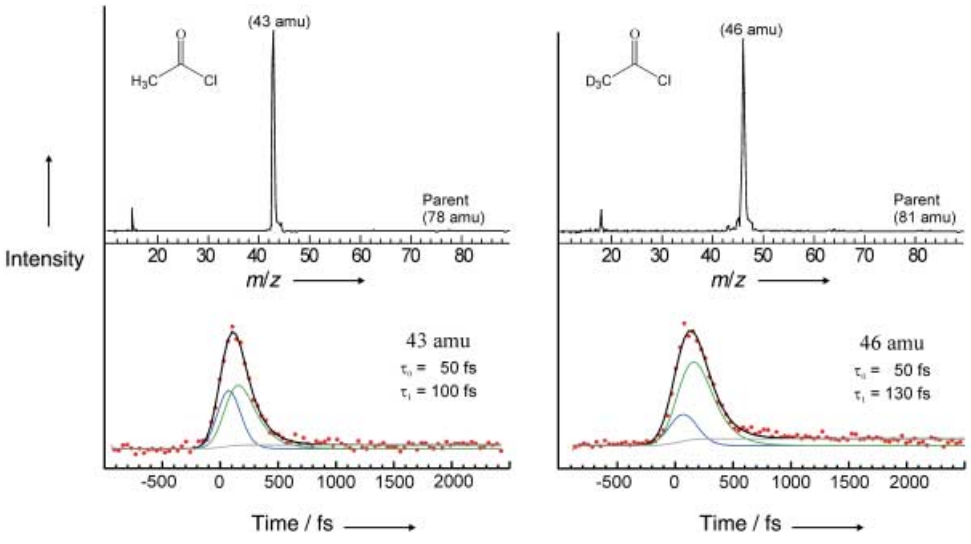

Figure 18. *Acetyl chloride and [D_3]acetyl chloride transients and MPI mass spectra. Note the absence of an isotope effect and the short timescale for the fragment decay. This behavior is very different from that of the acetyl fragments that arise from acetone and [D_6]acetone (see Figure 5).*

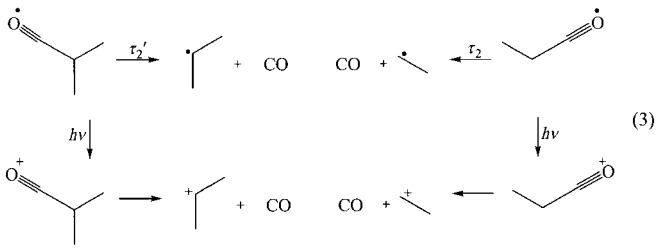

(3)

and then remains constant (alkyl radicals do not decompose easily); such a behavior was not observed.

In the case of MBK, a τ_2 value of 450 fs was derived from the transient recorded at $m/z = 57$. This time constant is significantly higher than the one derived from the parent transient and it can therefore not result from parent fragmentation alone. The appearance of the transient recorded at $m/z = 43$ offers an important piece of information regarding the identity of the species with the mass of 43 amu. From Figures 5 – 8, it can be seen that all the transients for the acyl compounds have a distinct appearance where the initial spike component is not very pronounced. This is not the case for the transient that corresponds to the fragment from MBK with a mass of 43 amu. In fact, the 43 amu transient in Figure 6 more closely resembles the alkyl cation transients (see the transients taken at $m/z = 29$ for MEK and DEK (Figure 3 and 7) and the transients taken at $m/z = 43$ for EPK and DPK (Figures 4 and 6)). We take this finding to indicate that the species of mass 43 amu that results from MBK does not correspond to CH_3CO^+ but to $C_3H_7^+$ which could be formed in decomposition of the *tert*-butyl cation. Because the 43 and 57 amu species are formed from the same precursor, the corresponding transients in turn give rise to the same time constant.

The result that the MPI mass spectrum of DBK (Figure 11) also has a peak at $m/z = 43$ supports the conclusion that the ion with the mass of 43 amu is formed from the *tert*-butyl cation. It is noteworthy that the time constant that correspond to the second bond breakage in the case of DBK (decomposition of the *tert*-pentanoyl radical) differs from the time constant that is obtained from the transient recorded for the fragment with the mass of 57 amu. The difference seems to be beyond the experimental uncertainty (Table 1). The obvious source of the fragment with the mass of 57 amu ($C_4H_9^+$) would be the decomposition of the C_4H_9–CO^+ acyl cation, but this scenario would result in identical time constants associated with the 57 and 85 amu transients. The results of our theoretical investigation indicate that for the first bond breakage the energy demand for the formation of an excited-state acyl radical and an excited-state alkyl radical is comparable when the alkyl radical is *tert*-butyl (Table 3). This would explain why DBK does not follow the trend of the remaining ketones under study and why the formation of the acetyl radical from MBK is negligible.

4. Dynamics of Norrish Type-I Reactions

4.1. General Mechanism

Based upon the combination of experimental and theoretical results reported here and in paper III, the general mechanism of Norrish type-I reactions can now be elucidated. For excitation to a high-lying state three elementary steps are involved. The dynamics are illustrated for acetone as the prototype; see Figure 13 and 15.

The initial step takes the wave packet down to the S_2 surface, which is the lowest of the Rydberg states that offers the prospect of C–C bond breakage at the available energy of $\sim$8 eV. This process of femtosecond internal conversion involves the *excitation center* (the carbonyl group) and is brought about by the C=O stretching motion and the conical intersections between the Rydberg and the valence $B_1(n_z \rightarrow \pi^*)$ states. Given the fact that the energy that is being transferred by the electronic excitation is located right where it is needed to activate the C=O stretch and given the efficiency of funneling through the conical intersections, the internal conversion from S_n to S_2 can be effectively achieved within a vibrational period of the CO stretch ($\nu \sim 1500\ cm^{-1}$). The process determines the magnitude of τ_0 and accounts for the femtosecond timescale observed here and for many other molecules at high energies. This fs motion is an efficient process, unlike conventional internal conversion between states utilizing a weak coupling and a high density of states.

The second step represents the first C–C bond breakage which occurs on the S_2 potential surface. The passage of the conical intersection (**CI2**) directs the energy into the asymmetric C–C stretching mode, which leads to a prompt bond breakage. This direction of reactivity is dictated by the nonadiabatic coupling vector of **CI2** (Figure 14). The passage of the barrier to form a methyl and an acetyl radical is what determines the magnitude of τ_1. The acetone molecule in the S_2 state correlates with an excited-state acetyl radical along the α-cleavage reaction coordinate. The unpaired electron resides in the 3s orbital and the equilibrium structure of this species is linear. Therefore the reaction coordinate also involves a significant in-plane bending motion.

The first bond breakage is highly nonstatistical in nature, as might have been anticipated on the basis of the partition of the available energy driven by the **CI2**. For example, τ_1 is largely unaffected by molecular size. It does become slightly larger as the size of the molecule increases but the effect is nowhere near as dramatic as one would expect from a statistical model such as RRKM theory. For example, upon increasing the molecular size, from acetone (10 atoms) to diisopropyl ketone (22 atoms), the rate should change by roughly eight orders of magnitude. Previously, we have shown that ring size does not affect the rate of Norrish type-I reaction on the femtosecond time scale, indicating that the distribution of internal energy in cyclic ketones is highly nonstatistical.[19, 20] Finally, the involvement of selective motion and not the entire phase space is consistent with the observation of the isotope effect for labeling at the α-position (not β-position), which reflects the involvement of the umbrella motion.

The final step is the further decomposition of the linear 3s acetyl radical ($3s\ ^2A'$). The measured time constant is much larger than that of the first bond breakage. As shown in Figure 15, this acyl radical decays to final products through two channels, either directly (σ^* character) to give products or by converting to the

bent configuration through **CI4**, which then decomposes to products. However, as shown in Figure 16, it is much easier to ionize the linear configuration over the bent one.

The phase space of the linear acyl radical involves the α-C–C bond breakage and, at least, the CCO bending motion. In Figure 19, we show a simplified sketch of the phase space.

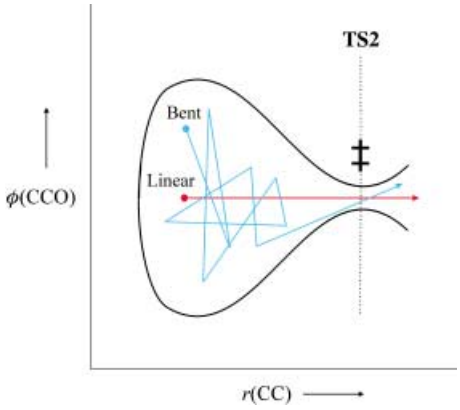

Figure 19. *A simple trajectory scheme representing the second CC bond cleavage dynamics of acetone. The slow and the fast motions are shown as blue and red trajectories, respectively. Note that the trajectories along the ϕ(CCO) bending coordinate are nonreactive while those along the r(CC) bond-stretching coordinate will immediately lead to bond dissociation through a narrow bottleneck (**TS2**); see text.*

Elsewhere, we have considered this problem with particular focus on the difference between wave packet localization and microcanonical preparation. Since the wave packet is not created precisely along the CCO coordinate, trajectory calculations[48] show the bifurcation of the wave packet in phase space—"direct" trajectories, mainly along the reaction coordinate, and "indirect" trajectories which involve motion first along the CCO coordinate. The former is on the less than 100 fs time scale, as it is dictated by the time scale to reach the transition state within a vibrational period along the C–C bond, while the latter is an IVR-type time scale and thus much longer than the former. In Figures 8 and 15 of ref. [48] are shown the results of such trajectory calculations and the proportion of direct and indirect trajectories, the dynamic consequences.

We therefore conclude that the observed hundreds of femtoseconds for this step is the time it takes for the trajectories, originally activated near the CCO bending coordinate (nonreactive), to enter the CC bond-breaking RC and eventually reach the **TS2** region. Note that the potential after **TS2** is repulsive in nature (σ^*) so that very efficient trajectories are expected to funnel into **CI4** and the subsequent bond-breaking reaction will occur on the ground-state PES. In contrast, the direct trajectories can lead to products in less than 100 fs, or to an intermediate, for example for cyclic ketones, which can further decay to final products. For example, for CP and [D_4]CP the observed transients taken at 28 and 30 amu (CH_2=CH_2 and CD_2=CD_2, respectively, Figure 20) clearly show a fast component and a slow decay component. This indicates that ionization of product trajectories may reflect some ionization of the direct trajectories of the

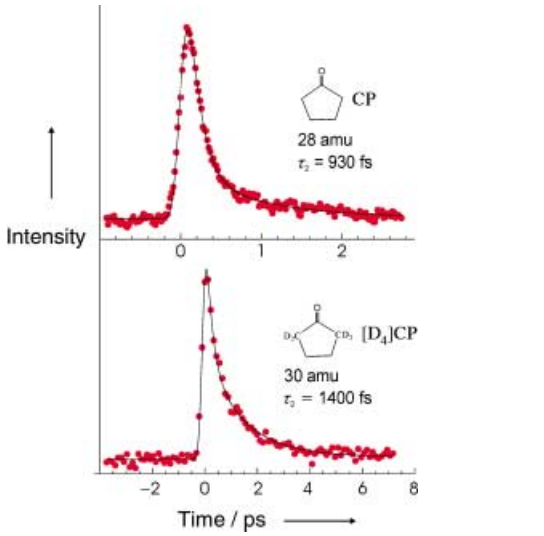

Figure 20. *Transients taken at 28 amu (cyclopentanone) and 30 amu ([D_4]CP). The experimental data points are given as red dots and the overall fit is shown as a black line. Note the difference in time scale from Figure 8 and 9.*

intermediate and not parent decomposition alone. Additionally, it is noteworthy that the τ_2 values derived from the transients shown in Figure 20 are larger than those obtained from the other fragment masses. This indicates that τ_2 in fact *is* larger and could possibly reflect the further decomposition of the tetramethylene diradical (the vertical ionization potential of this diradical is 7.55 eV, which we have calculated at the B3LYP/6-31G(d) level of theory); the final products of CP at $\sim$150 nm excitation are near 90% CO, ethylene, and cyclobutane (see ref. [19]). The uncertainty on τ_2 derived from the transients in Figure 20 is large because of the large amplitude of the rapidly decaying component. It should be noted that the ionization potential (Figure 16) of the linear excited-state acyl radical is independent of the CCO bending angle (as opposed to the bent ground state). Thus, trajectories of all phase space for the excited-state acyl radicals are probed.

Finally, we emphasize the contrast between the reactions on the ground- and excited-state potential energy surfaces. Norrish type-I reactions from the excited state involve the promotion of an electron in the nonbonding (n_y) orbital on oxygen. This is fundamental to the utilization of the reaction center in the formation of a new π-bond by overlap between the remaining unpaired n_y electron and the electron that becomes available when the α-CC σ-bond is broken because of the involvement of CO stretching and CCO bending motions (Scheme 1, paper III). On the ground-state surface the energy barrier is lower for the formation of the bent acetyl radical and there is no involvement of n_y electrons. Our ab initio calculations indicate that the products are formed through a unimolecular reaction ($CH_3CO^{\bullet}$ + $CH_3^{\bullet}$) and that the observed products in many thermal reactions (ketene and methane) are bimolecular secondary reactions. These findings are consistent with very recent infrared multiphoton dissociation studies by Berrie et al.,[17c] where it is shown that the thermal decomposition pathway of ketones in the dilute gas phase is unimolecular.

4.2. Applications

Real-time observations of the α-cleavage dynamics of acetone have been reported at various wavelengths covering excitations to the n_y,π^* state (S_1), the 3s Rydberg state (S_2), and highly excited Rydberg states (S_n). Since the S_1 dynamics of acetone has been detailed elsewhere,[11] we will now focus on discussing the S_2 and the S_n dynamics in the following Section.

4.2.1. Dynamics of Acetone (S_2) at 6.4 eV

Castleman and co-workers[8] studied the S_2 dynamics of acetone using pump – probe mass spectrometry at an excitation wavelength of 390 nm (3.2 eV) and a probe wavelength of 780 nm (1.6 eV). A stepwise reaction mechanism was reported and the corresponding time constants were determined to be 3.2 (6.0) ps and 1.7 (2.5) ps from the parent and the fragment-ion signals, respectively; results for the deuterated species are shown in parentheses. Using a similar pump – probe (194 – 388 nm or 6.4 – 3.2 eV) combination with a one-photon excitation energy almost identical to that of Castleman and co-workers,[8] Baronavski and Owrutsky[7, 9] reported the two time constants to be 4.7 (13.5) ps and 3.1 (3.0) ps from the parent and the fragment ion signals, respectively. Since the excitation in both cases are very close to the 3s 0-0 band, the available energy is not sufficient for the excited molecule to undergo either a direct surface crossing to the S_1 PES via **CI1** or a prompt first α-CC bond breakage on the S_2 PES via **TS1**. Therefore, the α-cleavage process takes place on the S_1 PES after a relatively slow $S_2 \rightarrow S_1$ internal conversion (IC) process. Scheme 3 summarizes the reaction dynamics of acetone upon excitation to the S_2 minimum region according to the above two experimental results.[7–9, 49]

$$S_0 \xrightarrow[(6.4\ eV)]{h\nu} S_2 \xrightarrow[IC]{3\ ps} S_1 \xrightarrow[-\ \cdot CH_3]{\sim 2\ ps} \text{Acetyl } (\tilde{A}^2A'') \xrightarrow{3\ ps} \text{Acetyl } (\tilde{X}^2A') \xrightarrow[-\ \cdot CH_3]{} P$$

Scheme 3. *Proposed mechanism and time constants for the α-cleavage process of acetone upon excitation to the S_2 0-0 region.*

There are two reasons for the assignment of the dynamics of each step shown in Scheme 3. First, the equilibrium structure on the S_1 and the S_2 state is quite different; S_2 resembles the ground state while S_1 is a different, with a pyramidal (CO bent out-of-plane) geometry. Therefore, the probe energy required to ionize the species from the S_1 state would be much higher than in case of the S_2 state.[50] Because of this change in geometry, two different ionization windows (at two different probes) can be invoked in the two experiments.[7–9] Second, the absence of the isotope effect on the second time constant of the Baronavski and Owrutsky study indicates that the corresponding process is not likely to involve a CC bond breakage, rather, it may be related to a nonadiabatic electronic transition ($\tilde{A}^2A'' \rightarrow \tilde{X}^2A'$) before the CC bond breakage occurs. The magnitude of the lifetime (3 ps) is on the same order as that of the excited-state HCO formyl radical ($\tilde{A}^2A''$).[51]

Along the CCO bending reaction coordinate, the acetyl ionization potentials between the neutral $\tilde{A}^2A''$ state and the cation ground state are very similar, whereas the ionization potentials (IPs) between the neutral and the cation ground states are dramatically different (Figure 16). Therefore, at least three probe photons of 3.2 eV are required to observe the ion signal corresponding to the $\tilde{X}^2A'$ species, whereas two photons suffice in the case of the $\tilde{A}^2A''$ species. This supports our assignment regarding the slow nonadiabatic transition of the acetyl radical (3 ps), because the ground-state CC bond-breaking process would then be probed only at a higher energy.

Another comment on the S_2 dynamics of acetone is the time scale of the subsequent α-cleavage on the S_1 PES after the $S_2 \rightarrow S_1$ IC process. The observed picosecond bond-breaking dynamics is consistent with our previous study for the S_1 dynamics of cyclobutanone above its bond-breaking threshold.[52] In the cyclobutanone case, the observed $\sim$5 ps α-cleavage dynamics is due to IVR at the available internal energy. Similarly for acetone upon excitation to the S_2 0-0 region, the b_1 CO out-of-plane bending mode must be activated on the S_1 surface due to the necessary vibronic coupling during the $S_2 \rightarrow S_1$ IC process. Therefore, IVR is an important process to be considered for the observed picosecond-scale α-cleavage dynamics taking place on the S_1 PES, especially when the available energy is above the bond-breaking threshold.

4.2.2. The Kinetic Energy Release—Decomposition of Acetone on the S_1 and the S_2 Surfaces

The measurements of the kinetic energy release that accompany the formation of acetyl radical, methyl radical, and carbon monoxide are particularly relevant. The results provide information regarding the distribution of the center-of-mass translational energy and the internal energy of the fragments during the α-cleavage reaction. Using the technique of molecular-beam photofragment translational spectroscopy (PTS), Lee and co-workers[17b] have found that the average kinetic-energy release ($\langle E_T \rangle$) upon excitation to the S_1 state ($\lambda_{ex} = 248$ nm or $E_{ex} = 115$ kcal mol^{-1}) is 14.2 kcal mol^{-1}, whereas the $\langle E_T \rangle$ is only 7.7 kcal mol^{-1} when the excitation is to the S_2 state ($\lambda_{ex} = 193$ nm or $E_{ex} = 148$ kcal mol^{-1}). Furthermore, the value of $\langle E_T \rangle$ at 248 nm is very similar to that measured at 266 nm ($\langle E_T \rangle = 13.9$ kcal mol^{-1})[53] regardless of a difference of $\sim$8 kcal mol^{-1} in the available energy. These results are somewhat counterintuitive because one may expect that more kinetic energy would be released when a higher excitation energy is used. However, the results can be rationalized according to the proposed dynamic model discussed in this paper.

In the case of excitation to the S_2 state near its 0-0 band ($\lambda_{ex} =$ 193 nm) as mentioned previously, the available energy is not sufficient for any reaction to occur from this state and the α-cleavage of acetone must take place on the S_1 PES after the $S_2 \rightarrow S_1$ IC process. This relatively slow IC process ($\sim$3 ps) allows for efficient distribution of the available energy ($\sim$60 kcal mol^{-1} above the S_1 minimum) into the internal degrees of freedom ($3N - 6 = 24$). The subsequent α-CC bond breakage could occur when the available internal energy is sufficient for the S_1 species to surmount the corresponding barrier ($\sim$0.8 eV or

$\sim$18 kcal mol^{-1}; Figure 15). Based on a statistical model for the first CC bond breakage on the S_1 PES, there will be $\sim$10 kcal mol^{-1} (25%, 6 out of total 24 degrees of freedom) of the total available energy ($\sim$42 kcal mol^{-1}) becomes translational while the rest ($\sim$32 kcal mol^{-1} or 75%) becomes internal energy of the two fragments (linear acetyl and methyl radicals). Note that an additional $\sim$20 kcal mol^{-1} internal energy will become available when the linear excited-state species ($\tilde{A}^2A''$) internally converts into the bent ground-state acetyl radical ($\tilde{X}^2A'$). Therefore, this is consistent with the fact that the second CC bond cleavage of the highly energetic ground-state acetyl radical occurs on a time scale which is much shorter than the flight time of the species to the time-of-flight detector,[17b] and hence the second bond dissociation occurs prior to the detection. Furthermore, the measured $\langle E_T \rangle$ of only 7.7 kcal mol^{-1} is also consistent with the release of kinetic energy during the first CC bond breakage on the S_1 rather than the T_1 PES, where the latter has a much higher exit barrier (the energy barrier with respect to the product channel).

However, when the molecule is excited directly to the S_1 state (near or slightly above the barrier) by $\lambda_{ex} = 248$ or 266 nm, the large fraction of the available energy partitioned into translation of the fragments suggests that the kinetic energy release is dominated by the exit barrier on the T_1 surface after the $S_1 \rightarrow T_1$ ISC process.[11, 17b] This mechanism is supported by the following two points. First, the PTS signal corresponding to the acetyl radical (mass 43 amu) was unambiguously observed at both wavelengths, indicating that the nascent acetyl radical must have a lifetime ($>$10 μs) long enough for the species to reach the detector before fragmentation. This is due to the fragment internal energy distribution involving the low energy portion. The energy barrier for the CC bond breakage in the ground-state acetyl radical was determined to be 17 kcal mol^{-1},[17a] so it is not possible to observe a stable acetyl radical with low internal energy if the first bond breakage occurs on the S_1 PES. Second, RRKM calculations predict the statistical α-cleavage reaction rate on the S_1 PES of acetone to be $\sim$0.2 ns^{-1} at 266 nm and $\sim$0.01 ps^{-1} at 248 nm. In both cases the reaction rate is slower than the time scale of IVR and randomization of the available energy must be taken into account for the first α-CC bond breakage on the S_1 PES. However, the partition of the available energy was found to be highly nonstatistical with a substantial fraction of the energy being translational, consistent with the α-cleavage occurring on the T_1 surface with substantial exit barrier; the $S_1 \rightarrow T_1$ ISC process is the rate-limiting step upon excitation to the S_1 state.

4.2.3 The One-Photon S_n Dynamics at 8 eV

Radloff and co-workers studied the S_n dynamics of acetone using femtosecond pump–probe mass spectrometry at the excitation wavelength of 155 nm (8.0 eV) and the probe wavelength of 387 nm (3.2 eV).[12] Two time constants were observed. The first component results from the parent ion and gives a time constant of 330 fs, and the fragment ion signal involves an extra offset component, which persists up to many picoseconds. These results are surprisingly different from ours using the similar technique at almost the same excitation energy (8.1 eV). We rationalize this result by the following scheme derived from our general picture: The $A_1(n_y \rightarrow 3d_{yz})$ state is involved by a one-photon excitation at 8.0 eV whereas the $B_1(n_y \rightarrow 3d_{xy})$ state (of the $B_1 - B_2$ pair in ref. [13]) is involved through a two-photon excitation at 8.1 eV; the corresponding mechanism is summarized in Scheme 4 and details are given in the following.

$$S_0 \xrightarrow[(8.0\ eV)]{h\nu} A_1\left(\begin{matrix}3d_{yz}\\ \pi\rightarrow\pi^*\end{matrix}\right) \xrightarrow[\text{trapping}]{\text{nonadiabatic}} \xrightarrow[\text{out-of-plane bend}]{330\ fs}$$

$$A'(n_z\rightarrow\pi^*) \xrightarrow[CI]{\text{ultrafast}} A'(\pi\rightarrow\pi^*) \xrightarrow{> 10\ ps} P$$

Scheme 4. *Proposed mechanism and time constants for S_n dynamics of acetone upon one-photon excitation at 8.0 eV.*

The one-photon absorption selection rules ensure that the a_1 CO stretch vibrational mode can be activated upon excitation to the $A_1(n_y \rightarrow 3d_{yz})$ state; the S_n dynamics of acetone along the CO bond-length coordinate is illustrated in Figure 21. The initial

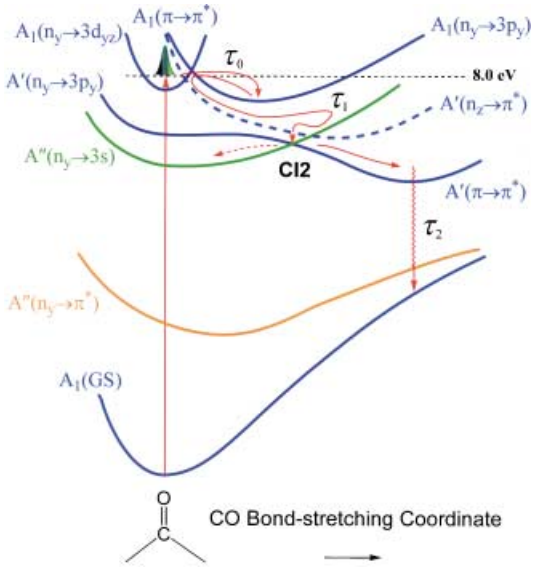

Figure 21. *The schematic representation for the S_n dynamics of acetone along the CO bond-stretching coordinate upon one-photon excitation at 8.0 eV (see text).*

wave packet on the $A_1(n_y \rightarrow 3d_{yz})$ PES efficiently transfers to the $A_1(\pi \rightarrow \pi^*)$ PES along the CO bond-stretching coordinate, due to the Rydberg–valence interaction by the efficient vibronic coupling between the two A_1 states. The coupling time (τ_0) is expected to be very short and the C_{2v} symmetry will be maintained during this process. This ultrafast coupling mechanism is supported by the evidence from the UV/Vis absorption spectrum of acetone[54] showing the underlying background signal in this energy region. The wave packet will be trapped between the $A_1(\pi \rightarrow \pi^*)$ potential well and the initial $A_1(n_y \rightarrow 3d_{yz})$ state and this "nonadiabatic trapping" effect is due to the strong Rydberg–valence interaction between the two A_1 states. At this

stage, the C_{2v} molecular symmetry is still retained and the coupling of the A_1 state with the other states of different symmetry is less effective.

The nonadiabatic trapping between the two A_1 states can be destroyed by breaking the symmetry from C_{2v} to C_s through the b_1 CO out-of-plane bending motion. Because the b_1 vibrational motion can effectively mix the $A_1(\pi \rightarrow \pi^*)$ with the nearby $B_1(n_z \rightarrow \pi^*)$, both are A′ states in C_s symmetry, the wave packet originally trapped on the $A_1(\pi \rightarrow \pi^*)/(n_y \rightarrow 3d_{yz})$ surfaces will now couple to the $A'(n_z \rightarrow \pi^*)$ state and cascade down to the $A'(\pi \rightarrow \pi^*)/(n_z \rightarrow \pi^*)/(n_y \rightarrow 3p_y)$ surfaces to search for the key conical intersection (**CI2**). Note that both the CO stretching and the CO out-of-plane bending motions are involved in this process. The overall nonadiabatic trapping time is then the observed 330 fs (τ_1).

Finally, after funneling through **CI2**, the wave packet will follow the gradient difference ($\boldsymbol{x}_1$) vector direction and reach the $A'(\pi \rightarrow \pi^*)$ minimum region at longer CO distances. Since the CO out-of-plane bending motion has been effectively activated to unlock the trapping, it is energetically unfavorable to reach the $A'(n_y \rightarrow 3s)$ PES at the shorter CO distances and find **CI1** to further cascade down to the S_1 PES.[16] For this reason, the observed persistent component with an undetermined time constant (τ_2) in the fragment transient could be due to the bent equilibrium $A'(\pi \rightarrow \pi^*)$ species undergoing slow relaxation process(es) to reach the lower-energy states.[55] The low probability of following the nonadiabatic coupling ($\boldsymbol{x}_2$) vector direction is expected because the key b_2 vibrational mode is inactive in the case of one-photon excitation. Thus, the key difference for such longer time dynamics in these one-photon experiments is the initial symmetry, which is totally symmetric (A_1) and does not allow for the femtosecond-scale asymmetric nuclear distortions.

5. Concluding Remarks

Here, we summarize only the general points which result from the experimental and theoretical work. More details are given in texts and in Section 4.

a) Norrish reactions from all excited states lead to α-cleavage primarily because of the n_y electron promotion (resulting in making a π-bond and breaking a σ-bond) and subsequent nuclear motions (CC, CCO, and CO) in the reaction center. The "repulsive" nature of the surface is established as due to interactions (transition states and conical intersections) and not due to a repulsive σ^* C–C bond rupture. In contrast, ground-state dissociation involves a bent configuration path and the high endothermicity to produce $CH_3CO^{\bullet}$ plus $CH_3^{\bullet}$ must be overcome to break the C–C bond.

b) The initial motion of the wave packet out of the Franck–Condon region and through the conical intersection to the S_2 state occurs in $\sim$50 fs or less. The system on this time scale acquires the asymmetric configuration to break the C–C bonds and this is the origin of the ultrafast ($\sim$50–150 fs) first bond breakage and the nonstatistical behavior. (On the other hand, an excitation which gives rise to an initial symmetric state—as in one photon excitation—could slow down such dynamics by trapping on valence states.) The observed isotope effect reflects the motion in a reduced subspace involving the umbrella motion of the α-carbon atoms. This clear isotope effect at the α- and not at the β-position supports the direct involvement of the motion in the RC and the breakage of the bond at the α-site. The motion of wave packets in such reduced space[56] is known to give a large isotope effect.[57]

c) The second bond breakage occurs on a longer time scale (hundreds of femtoseconds) and proceeds from the linear geometry of the acyl radical either promptly to form CO or after converting to a bent structure. The phase space of the linear geometry produces two types of trajectories, directly involving C–C motion and indirectly involving both the CCO bending and C–C stretching motion. The isotope effect is similarly influenced by the nuclear motion involving the α-carbon.

This work was supported by the Office of Naval Research. C.K., a Feodor Lynen Fellow from the Alexander von Humboldt Foundation, acknowledges the foundation and Caltech for support. T.I.S. acknowledges the Danish Statens Naturvidenskabelige Forskningsråd and the Denmark–America foundation for financial support.

[1] W. A. Noyes, Jr. in *Photochemistry and Reaction Kinetics*, Cambridge University Press, Cambridge, **1967**, and references therein.
[2] S. K. Kim, S. Pedersen, A. H. Zewail, *J. Chem. Phys.* **1995**, *103*, 477–480.
[3] a) S. A. Buzza, E. M. Snyder, A. W. Castleman, Jr., *J. Chem. Phys.* **1996**, *104*, 5040–5047; b) S. A. Buzza, E. M. Snyder, D. A. Card, D. E. Folmer, A. W. Castleman, Jr., *J. Chem. Phys.* **1996**, *105*, 7425–7431.
[4] T. Shibata, T. Suzuki, *Chem. Phys. Lett.* **1996**, *262*, 115–119.
[5] S. K. Kim, A. H. Zewail, *Chem. Phys. Lett.* **1996**, *250*, 279–286.
[6] S. K. Kim, J. Guo, J. S. Baskin, A. H. Zewail, *J. Phys. Chem.* **1996**, *100*, 9202–9205.
[7] J. C. Owrutsky, A. P. Baronavski, *J. Chem. Phys.* **1998**, *108*, 6652–6659.
[8] Q. Zhong, L. Poth, A. W. Castleman, Jr., *J. Chem. Phys.* **1999**, *110*, 192–196.
[9] J. C. Owrutsky, A. P. Baronavski, *J. Chem. Phys.* **1999**, *110*, 11 206–11 213.
[10] J. C. Owrutsky, A. P. Baronavski, *Chem. Phys. Lett.* **2001**, *333*, 36–40.
[11] E. W.-G. Diau, C. Kötting, A. H. Zewail, *ChemPhysChem*, **2001**, *2*, 273–293.
[12] P. Farmanara, V. Stert, W. Radloff, *Chem. Phys. Lett.* **2000**, *320*, 697–702.
[13] M. Merchán, B. O. Roos, R. McDiarmid, X. Xing, *J. Chem. Phys.* **1996**, *104*, 1791–1804.
[14] D. W. Liao, A. M. Mebel, M. Hayashi, Y. J. Shiu, Y. T. Chen, S. H. Lin, *J. Chem. Phys.* **1999**, *111*, 205–215.
[15] K. B. Wiberg, R. E. Stratmann, M. J. Frisch, *Chem. Phys. Lett.* **1998**, *297*, 60–64.
[16] E. W.-G. Diau, C. Kötting, T. I. Sølling, A. H. Zewail, *ChemPhysChem* **2002**, *3*, 57–78, immediately preceeding this paper.
[17] a) S. North, D. A. Blank, Y. T. Lee, *Chem. Phys. Lett.* **1994**, *224*, 38–42; b) S. W. North, D. A. Blank, J. D. Gezelter, C. A. Longfellow, Y. T. Lee, *J. Chem. Phys.* **1995**, *102*, 4447–4460; c) C. L. Berrie, C. A. Longfellow, A. G. Suits, Y. T. Lee, *J. Phys. Chem. A* **2001**, *105*, 2557–2562; d) K. A. Trentelman, S. H. Kable, D. B. Moss, P. L. Houston, *J. Chem. Phys.* **1989**, *91*, 7498–7513.
[18] a) E. L. Woodbridge, T. R. Fletcher, S. R. Leone, *J. Phys. Chem.* **1988**, *92*, 5387–5393; b) G. E. Hall, H. W. Metzler, J. T. Muckerman, J. M. Presses, R. E. Weston, Jr., *J. Chem. Phys.* **1995**, *102*, 6660–6668; c) D. J. Donaldson, S. R. Leone, *J. Chem. Phys.* **1986**, *85*, 817–824.
[19] S. Pedersen, J. L. Herek, A. H. Zewail, *Science* **1994**, *266*, 1359–1364.
[20] E. W.-G. Diau, J. L. Herek, Z. H. Kim, A. H. Zewail, *Science* **1998**, *279*, 847–851.
[21] A. H. Zewail, *Femtochemistry: Ultrafast Dynamics of the Chemical Bond*, World Scientific, Singapore, **1994**, and references therein.
[22] E. W.-G. Diau, S. De Feyter, A. H. Zewail, *J. Chem. Phys.* **1999**, *110*, 9785–9788.

[23] E. P. Hunter, S. G. Lias, *NIST Standard Reference Database Number 69* (Eds: W. G. Mallard, P. J. Linstrom), National Institute of Standards and Technology, Gaithersburg, MD, **1998**; http://webbook.nist.gov.
[24] W. J. Hehre, L. Radom, P. v. R. Schleyer, J. A. Pople, *Ab Initio Molecular Orbital Theory*, Wiley, New York, NY, **1986**.
[25] *Gaussian 98 (Revision A.9)*, M. J. Frisch, G. W. Trucks, H. B. Schlegel, G. E. Scuseria, M. A. Robb, J. R. Cheeseman, V. G. Zakrzewski, J. A. Montgomery, R. E. Stratmann, J. C. Burant, S. Dapprich, J. M. Millam, A. D. Daniels, K. N. Kudin, M. C. Strain, O. Farkas, J. Tomasi, V. Barone, M. Cossi, R. Cammi, B. Mennucci, C. Pomelli, C. Adamo, S. Clifford, J. Ochterski, G. A. Petersson, P. Y. Ayala, Q. Cui, K. Morokuma, D. K. Malick, A. D. Rabuck, K. Raghavachari, J. B. Foresman, J. Cioslowski, J. V. Ortiz, B. B. Stefanov, G. Liu, A. Liashenko, P. Piskorz, I. Komaromi, R. Gomperts, R. L. Martin, D. J. Fox, T. Keith, M. A. Al-Laham, C. Y. Peng, A. Nanayakkara, C. Gonzalez, M. Challacombe, P. M. W. Gill, B. G. Johnson, W. Chen, M. W. Wong, J. L. Andres, M. Head-Gordon, E. S. Replogle, J. A. Pople, Gaussian, Inc., Pittsburgh, PA, **1998**..
[26] A. P. Scott, L. Radom, *J. Phys. Chem.* **1996**, *100*, 16502 – 16513.
[27] L. A. Curtiss, K. Raghavachari, P. C. Redfern, J. A. Pople, *J. Chem. Phys.* **1997**, *106*, 1063 – 1079.
[28] J. I. Steinfeld, J. S. Francisco, W. L. Hase, *Chemical Kinetics and Dynamics*, 2nd ed., Prentice Hall, Upper Saddle River, NJ, **1999**.
[29] S. Pedersen, A. H. Zewail, *Mol. Phys.* **1996**, *89*, 1455 – 1502.
[30] J. D. McNeill, R. L. Lingle, Jr., N.-H. Ge, C. M. Wong, R. E. Jordan, C. B. Harris, *Phys. Rev. Lett.* **1997**, *79*, 4645 – 4648.
[31] For MEK, α-MEK, and β-MEK the S_1 barriers for methyl loss were found to be 16.9, 17.7, and 17.6 kcal mol^{-1}, respectively (TD-B3P86/6-311++G(d,p)//CASSCF(10,8)/6-31G(d)). For ethyl loss the barriers are slightly lower (13.8, 15.1, and 14.4 kcal mol^{-1}, respectively).
[32] a) A. B. King, *J. Chem. Phys.* **1965**, *42*, 3526 – 3536; b) J. T. B. Marshall, D. H. Williams, *Tetrahedron.* **1967**, *23*, 321 – 333; c) W. Carpenter, A. M. Duffield, C. Djerassi, *J. Am. Chem. Soc.* **1967**, *89*, 6167 – 6170; d) R. Brandt, C. Djerassi, *Helv. Chim. Acta* **1968**, *51*, 1750 – 1762.
[33] C. A. Brown, A. M. Duffield, C. Djerassi, *Org. Mass Spectrom.* **1969**, *2*, 625 – 630.
[34] a) P. Longevialle, *Rapid Commun. Mass Spectrom.* **1995**, *9*, 1189 – 1194; b) P. Longevialle, O. Lefèvre, *Rapid Commun. Mass Spectrom.* **1996**, *10*, 621 – 626; c) P. Longevialle, O. Lefèvre, N. Mollova, G. Bouchoux, *Rapid Commun. Mass Spectrom.* **1998**, *11*, 57 – 60.
[35] S. Hammerum, T. I. Sølling, T. Vulpius, unpublished results.
[36] S. Hammerum, K. Norrman, T. I. Sølling, P. E. Andersen, L. B. Jensen, T. Vulpius, unpublished results.
[37] a) X. Hu, W. L. Hase, *J. Phys. Chem.* **1989**, *93*, 6029 – 6038; b) W. L. Hase, R. J. Duchovic, *J. Chem. Phys.* **1985**, *83*, 3448 – 3453.
[38] F. W. McLafferty, F. Tureček, *Interpretation of Mass Spectra*, 2nd ed., University Science Books, Mill Valley, CA, **1983**, p. 141; F. W. McLafferty, F. Tureček, *Interpretation of Mass Spectra*, 2nd ed., University Science Books, Mill Valley, CA, **1983**, p. 179.
[39] S. Hammerum, *Mass Spectrom. Rev.* **1988**, *7*, 123 – 202.
[40] M. L. McKee, P. M. Mayer, L. Radom, *Eur. Mass Spectrom.* **1998**, *4*, 23 – 30.
[41] J. C. Traeger, C. E. Hudson, D. J. McAdoo, *Org. Mass Spectrom.* **1989**, *24*, 230 – 234.
[42] M. A. Robb, M. Garavelli, M. Olivucci, F. Bernard in *Reviews in Computational Chemistry, Vol. 15* (Eds.: K. B. Lipkowitz, D. B. Boyd), Wiley-VCH, New York, NY, **2000**, pp. 87 – 146.
[43] G. A. Gaines, D. J. Donaldson, S. J. Strickler, V. Vaida, *J. Phys. Chem.* **1988**, *92*, 2762 – 2766.
[44] D. J. Donaldson, G. A. Gaines, V. Vaida, *J. Phys. Chem.* **1988**, *92*, 2766 – 2769.
[45] S. A. Trushin, W. Fuss, T. Schikarski, W. E. Schmid, K. L. Kompa, *J. Chem. Phys.* **1997**, *106*, 9386 – 9389.
[46] S. De Feyter, E. W.-G. Diau, A. H. Zewail, *Angew. Chem.* **2000**, *112*, 266 – 269; *Angew. Chem. Int. Ed.* **2000**, *39*, 260 – 263.
[47] S. Deshmukh, J. D. Myers, S. S. Xantheas, W. P. Hess, *J. Phys. Chem.* **1994**, *98*, 12535 – 12544.
[48] K. B. Møller, A. H. Zewail in *Essays in Contemporary Chemistry: From Molecular Structure towards Biology* (Eds.: G. Quinkert and M. V. Kisakürek), Verlag Helvetica Chimica Acta, Zurich, **2001**, pp. 157 – 188.
[49] There are two apparent differencies between the two measurements (refs. [7] and [8]). First, the first time constant reported in ref. [7] (4.7 ps) is larger than that reported in ref. [8] (3.2 ps); that also applies to the time constant which corresponds to the second bond breakage (3.1 versus 1.7 ps). Second, in ref. [7] only a weak isotope effect was reported (3.0 versus 3.1 ps) for the second time constant, whereas the isotope effect reported in ref. [7] is significant (1.7 versus 2.5 ps). Because the probe energies are very different in the two cases (3.2 versus 1.6 eV), the above results can be explained by realizing two different detection windows. That is, the observed 4.7 ps dynamics from the parent ion may involve two consecutive steps, which in the other experiment were independently probed in the parent and in the fragment ions to give the corresponding time constants (3.2 and 1.7 ps). Note that the process corresponding to the second time constant ($\sim$3 ps) may be dark or unresolvable in the data analysis of ref. [8].
[50] The ionization potential of acetone is 9.7 eV from the ground state (S_2 minimum lies above the S_0 minimum by 6.35 eV). The cation energy at the S_1 equilibrium structure is calculated to be $\sim$10.9 eV from the ground state (S_1 minimum lies above the S_0 minimum by 3.77 eV). Therefore, the minimum ionization energies required to probe the ion signals from the S_2 and the S_1 states are estimated to be 3.35 and 7.1 eV, respectively.
[51] A. D. Sappey, D. R. Crosley, *J. Chem. Phys.* **1990**, *93*, 7601 – 7608.
[52] E. W.-G. Diau, C. Kötting, A. H. Zewail, *ChemPhysChem* **2001**, *2*, 294 – 309.
[53] G. Hancock, K. R. Wilson in *Proc. 4th Int. Symp. Molecular Beams*, Cannes, France, **1973**, pp. 511 – 533.
[54] L. O'Toole, P. Brint, C. Kosmidis, G. Boulakis, P. Tsekeris, *J. Chem. Soc. Faraday Trans.* **1991**, *87*, 3343 – 3351.
[55] The femtosecond mass spectrum of the one-photon excitation shows a fragment signal at 42 amu and the corresponding transient displays the same offset component as for the transient of the 43 amu signal. Because the structure of the equilibrium A′($\pi \rightarrow \pi^*$) species is highly bent ($\delta = 50^\circ$) with elongated CO distance (r(CO) = 1.64 Å), ionization with sufficient energy of this species would lead to both the 43 amu (CH_3CO^+) and the 42 amu ($(CH_3)_2C^+$) ion fragments. Note that the fragment signal at 42 amu is completely absent in the case of two-photon excitation (Figure 10).
[56] A. H. Zewail, *Angew. Chem.* **2000**, *112*, 2688 – 2738; *Angew. Chem. Int. Ed.* **2000**, *39*, 2586 – 2631.
[57] H. Gou, A. H. Zewail, *Can. J. Chem.* **1994**, *72*, 947 – 957.
[58] a) A. Nicolaides, A. Rauk, M. N. Glukhovtsev, L. Radom, *J. Phys. Chem.* **1996**, *100*, 17460 – 17464; b) S. Hammerum, *Int. J. Mass Spectrom. Ion Processes* **1997**, *165/166*, 63 – 69.

Received: June 13, 2001 [F 247]